frontiers | Frontiers in Built Environment

TYPE Original Research
PUBLISHED 05 August 2022
DOI 10.3389/fbuil.2022.917945



OPEN ACCESS

EDITED BY
Tori Tomiczek,
United States Naval Academy,
United States

REVIEWED BY
Cindy Palinkas,
University of Maryland, United States
David Cannon,
University of Michigan, United States

*CORRESPONDENCE
Jack A. Puleo,
jpuleo@udel.edu

SPECIALTY SECTION
This article was submitted to Coastal and Offshore Engineering, a section of the journal Frontiers in Built Environment

RECEIVED 11 April 2022
ACCEPTED 01 July 2022
PUBLISHED 05 August 2022

CITATION
Everett CL, Williams O, Ruggiero E, Larner M, Schaefer R, Malej M, Shi F, Bruck J and Puleo JA (2022), Ship wake forcing and performance of a living shoreline segment on an estuarine shoreline.
*Front. Built Environ.* 8:917945.
doi: 10.3389/fbuil.2022.917945



# Ship wake forcing and performance of a living shoreline segment on an estuarine shoreline

Cassandra L. Everett[1], Oscar Williams[1], Emma Ruggiero[2], Michael Larner[3], Rachel Schaefer[4], Matt Malej[5], Fengyan Shi[1], Jules Bruck[2] and Jack A. Puleo[1]*

[1]Center for Applied Coastal Research, University of Delaware, Newark, DE, United States, [2]Coastal Resilience Design Studio, University of Delaware, Newark, DE, United States, [3]Sustainable Coastal Solutions, Inc., North Falmouth, MA, United States, [4]Department of Civil and Environmental Engineering, Massachusetts Institute of Technology, Cambridge, MA, United States, [5]Coastal and Hydraulics Laboratory, US Army Engineer Research and Development Center, Vicksburg, MS, United States

Investigation of the effectiveness of Natural and Nature-Based Features (NNBF) for protecting shorelines from ship wake is increasingly important with continued development along the coast, especially when combined with sea level rise. Studies that investigate the wave energy dissipation capacity of different techniques and account for variation in context will lead to improvements and innovation in designed NNBF. Few studies have examined the performance of NNBF in protecting shorelines from ship wake. In this study of a low-sloping estuarine shoreline adjacent to a major shipping route, a natural design using coir logs and wooden staking was implemented in a T-head groin configuration. Pressure transducers and electromagnetic current meters were deployed over ~1.5 months to investigate the energy dissipation and velocity attenuation capabilities of the installation. Results indicate that ship wakes account for 25%–50% of the total daily energy impacting the shoreline at the study site. Peak background velocities are typically over 50% smaller than the largest ship wake velocities. Field data and results of the fully nonlinear Boussinesq model, FUNWAVE-TVD, indicate that the installation is capable of decreasing energy impacting the shoreline by 10%–80% and is effective over the lower 50% of the tidal range and when submerged up to twice its height. Elevation surveys of the site indicate accrual of sediment within the installation, suggesting wave diffraction patterns promoting further accretion at the site over time. Observations indicate that coir logs may be effective in reducing wave energy from ship wakes but may fail under storm conditions in a moderate fetch confined channel. Findings from this study illustrate the opportunities and challenges nature-based solutions face in addressing ship wakes, and their ability to protect shorelines under high energy stressors.

KEYWORDS

**ship wake, FUNWAVE-TVD, living shoreline, nature-based solution, coir logs, wave attenuation**

# 1 Introduction

Marshes and coastal wetlands along estuaries provide a buffer of protection against hydrodynamic forcing. Natural sediment transport in tidal waterways is affected by the tidal range and controls the development and erosion of marshes and shorelines (Ross et al., 2017). Growing pressures from sea level rise and reductions in sediment supply due to upriver development, combined with effects of ship wakes, influence shoreline morphology and alter the formation and subsistence of coastal wetlands (Syvitski et al., 2005; Brophy et al., 2019; Ezcurra et al., 2019). The inland regions of estuarine waterways lack defense against large wave events because they are primarily subjected to weaker forcing resulting from currents, tides, and small wind waves that are limited by the relatively narrow fetch and shallow bathymetry. The built and natural environment along these waterways will become increasingly susceptible to erosion with an increase in global mean sea level (Neumann et al., 2015). For example, it is estimated that 46%–59% of global coastal wetlands will be lost to 0.5 m of sea level rise, and up to 78% will be flooded by 1.1 m of sea level rise under normal and high projections for sea level rise by 2,100 (Spencer et al., 2016).

Estuarine waterway systems provide valuable shipping routes for inland cities and ports. Increased trade and economic activity (Almaz and Altiok, 2012) has influenced the growth of marine traffic and the necessity for larger ships to transport cargo. Increased large-vessel traffic amplifies the negative impacts of ship-generated waves (Schroevers et al., 2011), hereafter referred to as ship wakes or wakes. Ship movement displaces water, forcing it to flow in front of, around, and under the hull from bow to stern, analogous to a moving surface pressure disturbance (Soomere, 2006). A typical ship wake event consists of a group of low-frequency waves followed by high-frequency large-amplitude waves, and an ultra-low-frequency wave component (Herbert et al., 2018). Vessel length may be an important variable in the development of high amplitude wakes in confined channels (Scarpa et al., 2019).

Ship wakes, due to their higher energy content relative to wind-generated waves in a short fetch environment, have the potential to increase erosion along waterway shorelines (Verney et al., 2007; Soomere et al., 2009; Houser, 2011; Bilkovic et al., 2019; Styles and Hartman, 2019), and cause a variety of negative ecological effects including marsh degradation, wildlife disturbance, and light attenuation for local vegetation (Gabel et al., 2017; Bilkovic et al., 2019). Ship wake events typically produce waves with amplitudes greater than those of wind waves in fetch-limited waters and occur more frequently than storm surge events that produce waves of a similar size (Gabel et al., 2017). Ship wake events can also increase current velocities by an order of magnitude (Rapaglia et al., 2015), and can produce higher near-bottom velocities than wind waves of the same amplitude (Gabel et al., 2017), causing increased sediment suspension. In addition, extreme events and ship wake activity are a known cause of bank failure in fetch-limited environments, and the erosive potential of ship wakes increases with diminishing width in the waterway (De Roo and Troch, 2015). Suspended sediment concentration also increases during ship wake activity as compared to calm conditions before the wake (Safak et al., 2021). The increase in suspension is likely to lead to increased sediment transport under ship wakes relative to background wind-wave forcing (e.g. Safak et al., 2021).

Populations are increasing along coastlines, leading to high density coastal development and a need to protect onshore structures often with hard structures (Douglass and Pickel, 1999). As a conservative estimate, 14% of coastlines in the continental U.S. are hard armored, with the highest concentrations in cities (Gittman et al., 2015). Traditional structures like bulkheads starve estuarine shorelines of sediment (Zabawa et al., 1981) and lead to the loss of intertidal habitat (Douglass and Pickel, 1999). Hard structures prevent physical energy from impacting the shoreline onshore of their placement and help maintain shoreline position. However, they do not decrease the energy or erosion capacity of the wave environment offshore of the structure, allowing for continued erosion and elevation loss. In fact, the reflection of waves, including ship wakes, off of the bulkhead may increase the local energy levels. When compared to natural and restored shorelines, bulkheads may perform worse in protecting shorelines from erosion (Gittman et al., 2014; Smith et al., 2017) and have shown greater and more costly damages during hurricane events (Smith et al., 2017).

Research concerning natural alternatives to hard structure shoreline protection has increased rapidly since the term “living shoreline” was introduced in 2008 (Smith et al., 2020); where living shoreline is generally used to refer to shoreline protection strategies that include an element of habitat restoration (NOAA, 2015). Living shorelines have the potential to dissipate wave energy, stabilize shorelines, reduce flooding, and reduce the impact of large storms while providing co-benefits to ecological and economic systems (Temmerman et al., 2013; Davis et al., 2015; SAGE, 2015; O’Donnell, 2017; Kibler et al., 2019). The value of nature-based solutions is not well understood, especially in terms of coastal defense benefit, due to variations in materials, environment, and desired outcomes, and lack of research of different designs within these contexts (Gedan et al., 2011). Living shorelines are rarely monitored in the long-term for their effectiveness (Polk and Eulie, 2018; Bayraktarov et al., 2019) and those that have been implemented are not always intended to achieve coastal protection outcomes. Other measures of success, such as habitat creation, are often the primary focus of various investigations (Morris et al., 2018).

Living shorelines range widely in their ability to protect shorelines, require careful consideration of ecological components to ensure their sustained success, and may fail in

high energy conditions (De Roo and Troch, 2015; SAGE, 2015; Morris et al., 2018), such as ship wakes. The interaction between waves and living shoreline structures has shown successful wave dissipation by different designs (Meyer et al., 1997; Ellis et al., 2002; Dao et al., 2018; Safak et al., 2020a; Safak et al., 2020b; Mai Van et al., 2021), but requires further investigation. Few studies have examined the performance of living shorelines and natural and nature-based features in protecting shorelines from ship wake-induced erosion. However, shipping traffic can significantly alter the wave environment in low-energy waterways. Hydrodynamic processes and tidal depths play a vital role in the success of living shorelines installation such as low-crested brush bundle breakwaters (Ellis et al., 2002). Natural materials are chosen for accessibility, low cost relative to engineered materials, lack of interference with local ecology, biodegradability (impermanence in changing systems), and/or their permeability for wave dissipation as opposed to reflection. However, the applicability of these materials in different contexts is not well researched. In Delaware, and according to the Delaware Department of Natural Resources and Environmental Control (DNREC), "conventional living shorelines" are those employing natural materials, of which coir logs and oyster shell are the most common materials, and are typically constructed in lower energy areas (Delaware Department of Natural Resources and Environmental Control, 2020). Coir logs are accessible, low cost, handleable (low weight), and flexible in terms of application to project configurations. They typically break down in two to five years and are often used to establish a slope of ground elevation through accretion that supports plant material along a gradually sloping shoreline. Oyster shell is used to dissipate wave energy and establish a living breakwater by recruiting live oysters to establish a reef. Therefore, part of this study includes investigating such material recommendations in moderate energy systems. The aim of this study is to quantify the relative importance of ship wakes in the Delaware estuary and develop and test a low-cost nature-based living shoreline in a ship wake-influenced area. Investigating the behavior of such a structure composed of natural materials in an environment with heavy commercial shipping traffic will contribute to the growing body of knowledge surrounding living shoreline design.

# 2 Ship wake field and numerical study

## 2.1 Study site

The Delaware River is one of the most commercially navigated estuarine systems on the East Coast, serving as a major artery for over 40 ports and anchorages. About 3,000 ships traverse the waterway each year, supplying and exporting goods to and from major cities such as Camden, Philadelphia, Wilmington, and Trenton (Almaz and Altiok, 2012). The river is subjected to flood dominant semidiurnal tides as far inland as Trenton, limiting the passage of larger and deeper draft ships during low tides. Dredging projects since 2002 have increased the channel depth to 15 m to accommodate larger ships and increased shipping traffic (Cook et al., 2007).

Pea Patch Island is a silt deposit-formed island located on the Delaware River about 1.4 km east of Delaware City and about 1.6 km west of Fort Mott State Park (39°35.67′N, 75°34.35′W, Figure 1A). It has an average elevation of 1.38 m relative to the North American Vertical Datum of 1988 (NAVD88; mean water level is 0.85 m NAVD88) and roughly 95% of the island is less than 2.25 m in elevation. Pea Patch Island has a total area of about 1 $km^2$, with a length of ~1.9 km and a width of 0.8 km at its widest point. The small island is the site of Fort Delaware, a historic military fort, as well as the largest wading bird nesting area on the East Coast north of Florida. Historically, Pea Patch Island has been susceptible to shoreline erosion due to its location in the middle of the river near the shipping channel and has been the subject of many ongoing shoreline protection efforts to preserve the cultural history of the site and facilitate the roughly 30,000 annual visitors touring the island hosted by the Delaware State Parks (USACE, 2009).

The installation location is on the east side of Pea Patch Island (Figure 1B) adjacent to the main shipping channel, where the shoreline experiences severe erosion as evidenced by exposed tree roots. The river at this location is 1.6 km wide and more than half of this width is spanned by the channel of interest at 900 m wide (Figure 1C). The shipping lane within the channel is approximately 250 m wide and has navigational depths of 10–15 m. The channel runs closest to the shore along the southeastern side of the island and distance between the channel and the island shoreline increases farther north. At the installation location there is a silty-mud tidal flat that spans roughly 140 m between the channel and the shoreline. The tidal flat widens to the northwest and contains sandy shoals offshore.

Wetlands and shorelines are dynamic protection mechanisms for inland areas. A rising concern is whether Pea Patch Island will be able to adapt fast enough to the acceleration of external forces. Increased shipping traffic in the channel, sea level rise and increased storm intensity will result in growth of the mean annual wave power density. Wave power density may be directly proportional to the volumetric retreat of marsh edges (Marani et al., 2011). Shoreline retreat and cross-shore sediment transport result in a decrease in foreshore slope to dissipate wave energy (Dean and Dalrymple, 2002). However, continual dredging of the Delaware River channel decreases frictional forces and increases tidal amplitude resulting in faster tidal (alongshore) currents (van Maren et al., 2015; van Rijn et al., 2018; Ralston et al., 2019). The increase in alongshore currents removes suspended sediment from the local system. The shoreline south of the study site was armored with stone to

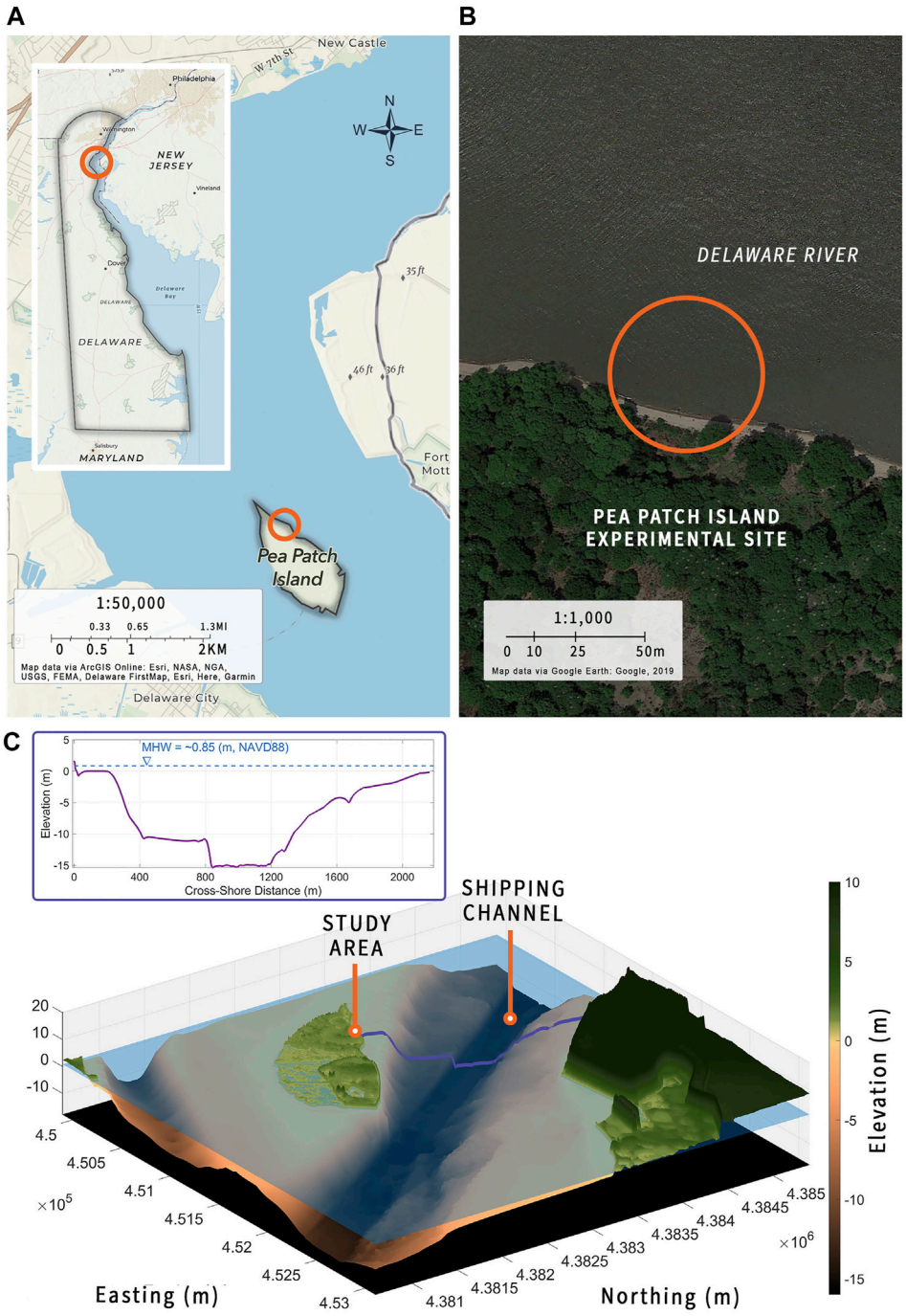


FIGURE 1
**(A)** Location of Pea Patch Island in the Delaware River. **(B)** Area of living shoreline and field instrumentation deployment. **(C)** Bathymetry in the shipping channel surrounding Pea Patch Island The subplot indicates the elevation of the cross-shore transect from the study site through the shipping channel.

protect the Fort. The protection creates a deficit in downdrift sediment transport upriver, and recent observations have shown erosional flanking at the lateral ends of the structure (Tait and Griggs, 1991; Schaefer, 2019). Moreover, an abrupt change in alongshore sediment transport causes beach erosion (Komar, 1998). The armoring around the Fort induces this type of abrupt

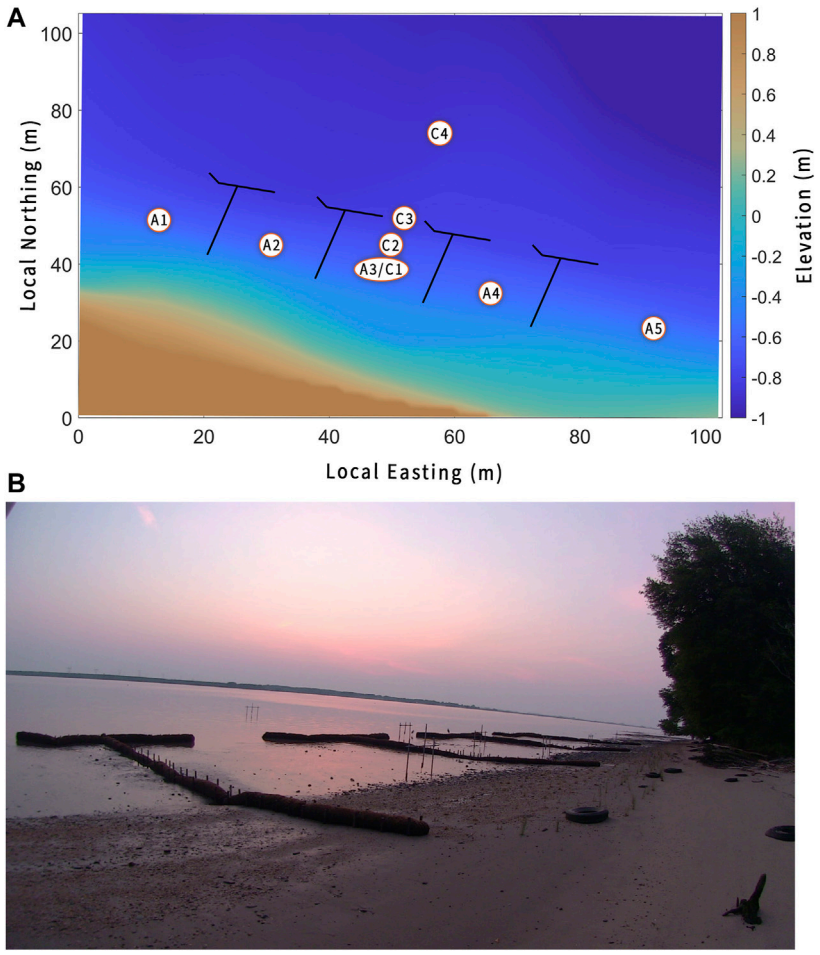


FIGURE 2
**(A)** Location of the study site in a local coordinate system with the layout of coir log THGs and locations of the deployed sensors. **(B)** Installed coir log THGs at Pea Patch Island. Photograph from Erdman Video Systems, Inc. livestream camera.

change in alongshore sediment transport and disrupts the island's natural ability to keep pace with sea level rise and increased shipping traffic.

## 2.2 Field study design and deployment

Two pilot field studies were conducted to test the feasibility of using coir logs and matting, wood or branch bundles, and oyster shells as natural materials within the context of the Pea Patch Island wave environment. In October 2020, a week-long pilot test consisting of staked single coir logs and staked modified coir logs with an oyster shell core were installed at the study site. These implements were tested at two different distances from the shoreline to determine qualitatively the depth dependence of a coir log breakwater as a shoreline protection strategy. Pilot testing revealed that the coir logs decreased wave height and wave energy impacting the shoreline (Baldauf, 2021). In November 2020, following these results, a T-head groin (THG) configuration consisting of coir logs with a wood bundle breakwater head was constructed using onsite driftwood. Recycled oyster shell bags were used to line the coir logs. The THG configuration was based on a similarly designed living shoreline in Vietnam composed of bamboo bundles (Albers and Schmitt, 2015). While the brush bundle breakwaters did not perform effectively in the environment at the pilot study site (excessive buoyancy and failure due to repeated rubbing of sisal twine), a THG configuration of coir logs was deemed appropriate for use under these conditions using field data and model simulations. Results of the pilot studies demonstrated dissipation capacity of natural

materials, as well as the failure of these materials to stay in place, likely due to insufficient anchoring.

Feedback from pilot studies was incorporated into a final design (Figure 2A) receiving a statewide permit on 8 April 2021 and was installed on 17–18 June 2021. The constructed living shoreline segment (Figure 2B) consisted of four THGs spanning ~65 m of beach. The westernmost coir log of the head of each THG was set at an angle of 45° clockwise from the centerline of the head of the THG. This modification was made to address the visually observed obliquely incident wakes produced by northbound ships. Each groin consisted of two 0.4 m (16 in.) diameter coir logs, placed farthest onshore, and eight 0.5 m (20 in.) diameter high density coir logs. The coir logs at the heads of the THGs were wrapped in jute matting to further protect them from the high-energy ship wakes. All coir logs were anchored using 0.05 m (2 in.) × 0.05 m (2 in.) × 2.44 m (8 ft.) oak stakes driven by a gas-powered post driver and secured with sisal twine using one-way square knots.

A field experiment was conducted from July 2 to 12 August 2021 (Figure 2). A cross-shore transect was established through the center of the installation that spanned from 22.7 m offshore from the heads of the THGs to 6.1 m offshore, at the onshore ends of the THGs (in line with the offshore end of the most onshore coir log). Additionally, an alongshore transect was established from 9.4 m northwest of the installation, with stations halfway between each pair of THGs, extending 18.2 m southeast of the installation. A5 and C4 were located to approximate tidal and wave conditions unaffected by the structure, while A1 was located to approximate the effects of being sheltered by only one THG. Note that ship wakes rarely reach the foreshore/berm during low tides and this study focused primarily on the propagation of waves and dissipation of energy across the THGs. The draft of ships is restricted to less than 12 m during low tides causing larger and more heavily loaded ships to work around the tide or transfer cargo to lightering barges (Almaz and Altiok, 2012). Wind speed and direction data were obtained from National Oceanic and Atmospheric Administration's (NOAA) National Ocean Service Physical Oceanographic Real Time System Program Station DELD1 Buoy at Delaware City, DE.

Eight stations were occupied and numbered C1–C4 in the cross-shore direction and A1–A5 in the alongshore direction (Figure 2A). C1 doubled as A3. Each station included a structure made from galvanized steel and aluminum pipes pounded into the sediment. Water depths were recorded with RBR Ltd. compact pressure transducers (RBRs). Two additional RBRs were placed above the high-water line to record atmospheric pressure. Fluid velocities at each station were recorded with JFE Advantech Co., Ltd. INFINITY-EM AEM-USB custom two-dimensional electromagnetic current meters (JFEs). RBRs and JFEs were deployed initially at 0.01 and 0.1 m above the bed, respectively. Battery life for the JFEs is approximately three days, resulting in the need for four deployments over the course of the study: July 2–4 July 2021, July 15–17 July 2021, July 20–22 July 2021, and July 29–31 July 2021. Battery life for the RBRs is approximately 30 days, resulting in the need for two deployments over the course of the study: July 2–19 July 2021 and July 20–12 August 2021.

The JFEs sampled continuously at a rate of 5 Hz. Velocity data were used to compare alongshore and cross-shore components and magnitudes among ship wakes and against background forcing. The RBRs sampled continuously at a rate of 2 Hz (A1, A5, C2, C3) or 16 Hz (A2, C1/A3, A4, C4). A Brinno TLC 200 PRO time lapse camera was deployed near the installation to record an image every 10 s. Additionally, a 1080p livestream camera with 3x zoom powered by solar panel from Erdman Video Systems, Inc., was placed on the northwestern end of the site to record an image every 1 min. The cameras captured ship passages, ship wakes, and tidal fluctuations and were used as a preliminary technique for identification of ship wake events.

Elevation surveys of the project area and a cross-shore transect through the center of the installation were collected in May (pre-deployment) and September (post-deployment) 2021 using a Leica Global Navigation Satellite System (GNSS) real-time kinetic global positioning system (RTK GPS), referenced to UTM zone 18 and NAVD88. Measurements were taken at intervals of ~5 m in the alongshore direction and ~1 m in the cross-shore direction. Vertical error in the elevation data is estimated as 0.05 m due to GPS system accuracy and the silty substrate.

## 2.3 Data processing

### 2.3.1 Depth and energy flux data

Pressure data were adjusted for atmospheric pressure and then water depth was estimated as:

$$d = \frac{P}{\rho g} \tag{1}$$

where $d$ is local depth in meters, $p$ is the measured pressure in Pascals, $g$ is the gravitational acceleration constant (9.81 m/s$^2$), and $\rho$ is an average water density for the Delaware River Estuary in kg/m$^3$ calculated using the International one atmosphere equation of state of seawater (Millero and Poisson, 1981). Salinities in the Delaware River Estuary range from 0.5–19 ppt (PDE, 2012) and the average temperature obtained from the offshore electromagnetic current meter (C4) was ~24°C. A range of densities was established (994.2–1,013.1 kg/m$^3$) and a typical density for brackish water of 1,013 kg/m$^3$ was selected. Using the lower bound of the density range increased the depth by 0.01 m, within the error range of the RBRs. Measurements were taken in shallow water, where dispersion is minimal, so Eq. (1) is a reasonable estimate for both long and short waves.

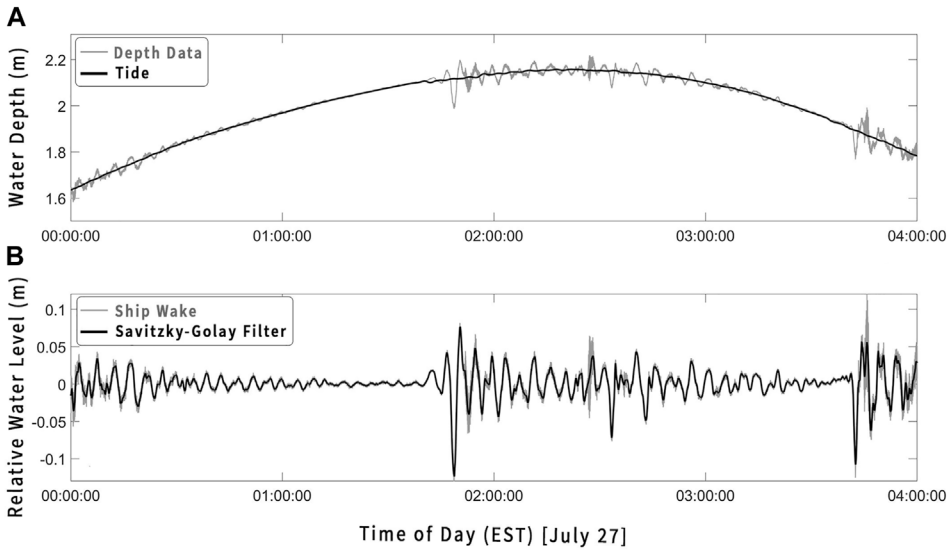


FIGURE 3
**(A)** Raw depth overlaid with computed tidal signal. **(B)** Depth data after tidal removal overlaid with Savitzky-Golay filtered data.

The tide signal was estimated from a time series of depth measurements using a running average filter with a 15-min window (Figure 3A). The demeaned tidal trend from C4 was used to identify the local water depth for each wake event. The high- and low-frequency signals generated by the ships were isolated by applying a Savitzky-Golay finite impulse response (FIR) convolution filter of polynomial order 10 and a frame length of 100 s to the residual time series (Figure 3B). The Savitzky-Golay filtered data were subtracted from the tide-removed data to separate the high-frequency signal from the low-frequency signal.

Approximate start times for each wake event were identified using time lapse video. The peak water elevation preceding the initial drawdown and a 20-min window of the subsequent data was retained. Data were catalogued chronologically by when the ship travelled past the island for subsequent identification. A 20-min window was chosen by inspection such that only small amplitude seiching on the order of background conditions remained visible in the signal.

Individual wave heights and periods in ship wakes were estimated differently for the low and high-frequency signals, due to the elevated water level in the low-frequency wake. Small amplitude (< 0.02 m) oscillations were neglected based on observations of typical wind wave amplitudes at the site. High-frequency waves (on the order of background conditions, with a typical period of < 5 s) were identified using the zero down-crossing method. Low-frequency waves (typical period of > 100 s) were identified by retaining successive local extrema with differences in water level greater than 0.02 m. Wave periods were taken as the time difference between successive troughs.

Wave energy density per unit surface area (Joules per square meter) can be estimated using small-amplitude linear wave theory as (Kamphuis, 2010):

$$E = \frac{1}{8}\rho g H^2 \tag{2}$$

where $E$ is the energy density and $H$ is the wave height. Wave power, or wave energy flux, per unit crest length (Watts per meter) can be estimated roughly as the energy density per unit surface area multiplied by the group velocity $C_g$ (Kamphuis, 2010):

$$F = EC_g = \frac{1}{2}EC\left(1 + \frac{2kd}{\sinh(2kd)}\right) \tag{3}$$

where $F$ is the wave energy flux, $C$ is the wave celerity (estimated as the wavelength divided by the wave period), and $k$ is the wave number. The wavenumber and wavelength were determined using the Newton-Raphson method to solve the dispersion relationship where the inputs were local water depth and the period identified in the filtered signal. Estimates of wave energy density and wave power using linear wave theory have been used previously to quantify the erosive potential of ship wakes (Gharbi et al., 2008). Percent decrease of energy fluxes between stations was calculated to estimate the relative efficiency of the installation.

### 2.3.2 Velocity data

Velocity data were removed from the record when the water depth was below 0.35 m, where a conservative 0.35 m rather than 0.1 m cut-off was used to account for the size of the measurement

portion of the sensor, sensor hysteresis upon intermittent submergence under wave activity, and the potential for GPS error due to unconsolidated silty-mud (where sensor elevation was determined using bed level elevation from RTK GPS). Acceleration magnitudes were calculated using a forward difference and a 98th percentile cut-off was established. Velocities were removed from the record when acceleration magnitude was greater than this cut-off or the velocity magnitude was greater than 0.5 m/s, which was the upper bound of the remaining ship wake velocities. For each wake, positive (offshore or southerly-directed) and negative (onshore or northerly-directed) velocities were separated and a 98th percentile velocity (peak) and mean velocity were calculated for each in the cross-shore and alongshore direction. The same percentile calculations were performed for background conditions after removing ship wake velocities.

## 2.4 FUNWAVE-TVD

FUNWAVE-TVD, a nonlinear Boussinesq wave model, was used to simulate wake conditions. This model contains a ship wake module added to the existing Boussinesq formulation, modelling vessels as a moving pressure source (Shi et al., 2018). The model was validated (Shi et al., 2018) using laboratory data (Gourlay, 2001) examining supercritical wake in various flow regimes including slow-moving, large container ships (Forlini et al., 2021). The model was first used to inform installation design by simulating conditions with and without the THGs, comparing maximum velocities and water surface elevations (Williams, Forthcoming 2022). Model bathymetry was collected in 2012 and altered with subsequent data collected in 2018, 2020, and 2021. The data include low tide surveys using GPS and channel bathymetry from the United States Army Corps of Engineers (USACE). The domain spans ~4,812 m in northing and ~3,207 m in easting with grid spacing of 1.3 m (easting) by 1.7 m (northing). Coir logs were added to the bathymetry by raising the bed 0.4 and 0.5 m at the locations where the respective sized coir logs were located. Simulations showed a reduction of maximum velocity and maximum water level onshore of the THGs.

### 2.4.1 Automatic Identification System data

A log of all large commercial ships that navigated the Delaware River from July 9 to August 12 was provided by the Maritime Exchange for the Delaware River and Bay. The log was generated using the United States Coast Guard's Automatic Identification System (AIS) containing records of ship specifications and time stamps when entering a waterway or port. Each ship will have at least three recordings per visit to the waterway, one upon entry, one for arrival at the port of destination, and one upon exiting the waterway. Often ships will have more than three recordings, accounting for anchorage stops and lightering locations.

Analysis of the timelapse footage revealed 680 ships passing the area (341 northbound and 339 southbound) during the study period, at a rate of ~16 ship passages per day. AIS data were filtered to retain nonstationary commercial vessels by neglecting vessels with a speed of 0 m/s, a draft less than 5 m, or a length less than 100 m. The timelapse footage results and AIS data were compared to match vessel data to individual wake events. Events during which the wake signal would be significantly altered, such as a second vessel passing within the 20-min analysis window, were neglected for the subsequent analysis, leaving 147 wake events.

AIS data including vessel length, width (or beam), draft, and course were then used to force individual ship passages in the model. However, AIS data report maximum vessel drafts. So, the drafts were adjusted to optimize model performance. Simulations lasted for 20 min of field time, a typical time from the start of a wake event to the return to background conditions.

### 2.4.2 Model validation

The model was validated using measured water levels. Key factors in model validation are the magnitude of maximum drawdown and subsequent surge (commonly referred to as the transverse stern wave) and the amplitude of the Kelvin wake. The phasing of the field data was not well modeled using the AIS course data. This mismatch is likely due to incongruencies between the modeled and actual bathymetry. Thus, for validation purposes, the phasing of the events was matched using the point of maximum drawdown as a reference point.

Model tests were performed separately for a chosen northbound and southbound ship wake event, due to the differences in their wake profiles. As previously mentioned the ship draft was adjusted to optimize model performance (Williams, Forthcoming 2022). The model accurately predicted the magnitude of peak drawdown within 4.0%, magnitude of peak subsequent surge within 3.6%, and the amplitude of the seiche within 1.4% for a northbound ship wake (Figure 4). The phasing between drawdown and surge was incorrect by 43 s. However, the south bound wake simulations were less successful (not shown). Drawdown and surge were predicted within 14.9% and 16.9%, respectively, but the southbound ship wake signal contains a higher frequency, high amplitude (~0.18 m) component, representing some of the largest waves observed, that the model does not predict. This component may be due to model inability to account for a tidal current and inconsistencies between the modeled and real bathymetry. For example, sand shoals to the north of the island, not well-represented in the model bathymetry, could alter wave patterns. The unmodeled high-frequency component also

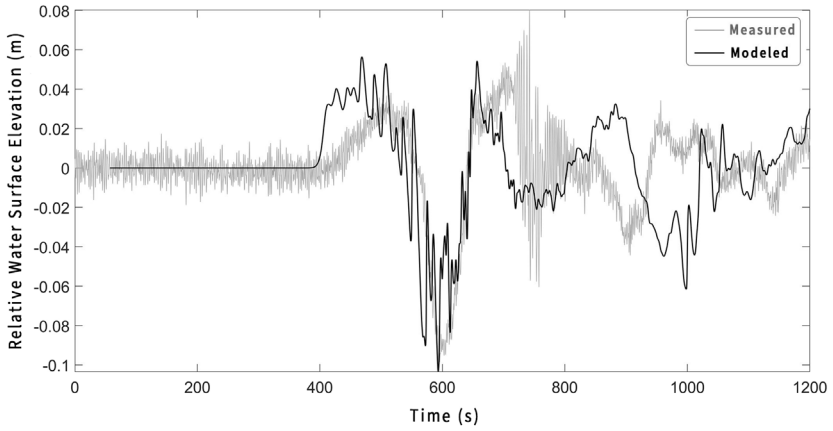


FIGURE 4
Comparison of measured and modeled surface displacements during wake event generated by northbound vessel JS Ineos Intuition.

exists in the northbound case (Figure 4), but with a smaller amplitude relative to the low-frequency drawdown and surge. De Roo and Troch (2015) note that for commercial shipping vessels, the drawdown and surge, rather than the higher frequency Kelvin wake, tend to contain the majority of the wave energy within a ship wake event. The inability to reproduce the high-frequency component is less detrimental to the northbound validation and further numerical analysis was performed only for a northbound ship wake event. The model was subsequently used to test the efficacy of the installation, as well as the effect of water level on the installation performance.

# 3 Results

## 3.1 Field conditions

The meteorological conditions during the study period were mild with a maximum wind speed of 11 m/s from the E and an average wind speed of 2.3 ± 1.4 m/s, predominantly from the SW (Figure 5A). The beach was sheltered from most of the wind influence from the SW. Conversely, the strongest wind influences from the E and NE directly impacting the beach had the longest fetch, despite being infrequent and duration limited. Typical background significant wave heights and periods at the site, taken as the significant wave height and period during all periods of no ship activity, range from not detectable to 0.06 m and 1.5 s (C4), respectively.

The beach profile in Figure 5B cross-shore bathymetric transect through the center of the installation, exhibits a slope of ~1:8 shoreward of the toe of the foreshore and a gradual slope of ~1:100 from the toe of the foreshore towards the channel. The profile shows a change in slope at an elevation of −0.51 m (NAVD88). At this location, ~12 m in the local cross-shore coordinate system (Figure 5B), there is also a change in the observed typical grain size from sandy to gravel/cobble to silty-mud. The cross-shore location of the slope break remained approximately the same over the study duration. The tidal range is ~1.7 m for this micro-tidal beach. The average high tide was 1.4 m above the toe of the foreshore (Figures 5B,C), indicating that wave breaking occurs mostly offshore of the installation. The average low tide was 0.3 m below the toe of the foreshore.

Elevation data were interpolated to a uniform grid (Figure 6) using smoothing scales of 5 m (Plant et al., 2002). Changes in elevation over the short timescale of the study were difficult to quantify from the individual surveys (Figures 6A,B). The elevation difference between the May and September surveys (Figure 6C) shows only small magnitude changes. In general, there was erosion directly behind the heads of the THGs (< 0.1 m ± 0.05 m) and accretion of similar magnitude farther onshore. In addition, there was more area of erosion between the two eastern THGs that gradually transitioned, moving west, to more area of accretion between the western THGs. Directly onshore of the three eastern THGs, there was accretion up to ~0.2 ± 0.05 m. There was erosion of a similar magnitude onshore of the western T, which can likely be attributed to the loss of the farthest shoreward coir log in an early September storm (see Section 4).

## 3.2 Wave characteristics

Data revealed that ships with deep drafts traveling in this confined waterway produce a fairly consistent wave signal

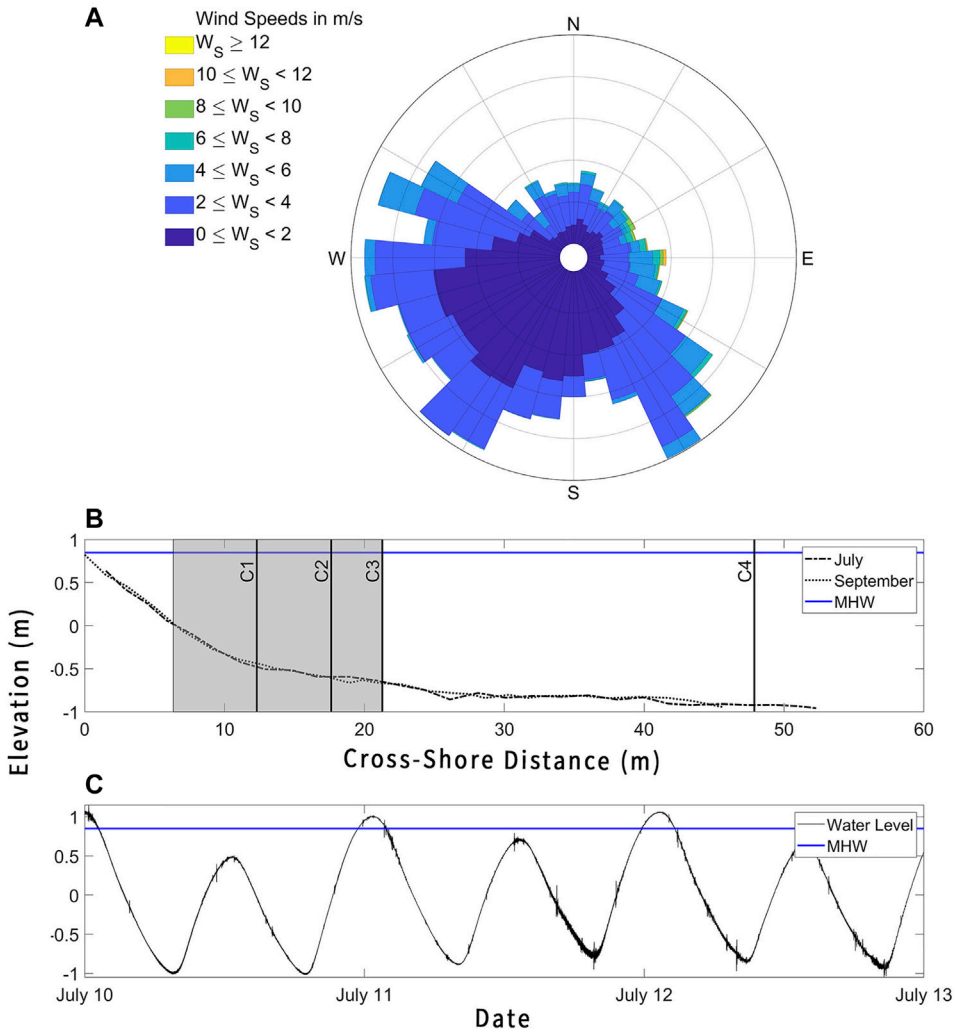


FIGURE 5
**(A)** Wind rose using data collected 10 times hourly from NOAA buoy DELD1 from 2 July 2021 to 12 August 2021. **(B)** Cross-shore bathymetric transect through the middle of the installation. July (September) denoted by dashed (dotted) black line. Installation delimited by shaded area. Stations denoted by solid lines and labelled. **(C)** Sample water level (NAVD88) data denoted by black line. Mean high water line denoted by blue line in **(B)** and **(C)**.

compared to the wakes generated by other vessels and natural wave conditions (Figure 7). Initially, a slight increase in water level travels along with the passing of the ship. The initial pulse is immediately followed by a substantial drawdown in water level resulting in a surging runup minutes after the ship has passed. The typical period of this drawdown and surge is approximately three to four minutes making it a low-frequency oscillation compared to other ship-induced wakes and wind waves. The low-frequency oscillations are followed by a high-frequency diverging and transverse wave train (Kelvin wake), the amplitude of which is related to ship geometry and speed. The drawdown and surge is followed by low-frequency seiching of smaller magnitude in addition to high-frequency wake. The period of harmonic mode one of the seiche as estimated by Merian's formula (Proudman, 1963) is 200 s–400 s. The seiche gradually decays in wave height due to the frictional forces acting upon the waves (Kamphuis, 2010). The combined drawdown and surge wave can reach heights greater than 0.3 m with seiche wave heights typically less than 0.1 m (Figures 7E,F). High-frequency waves (typical period < 5 s; Figure 7D) can reach heights greater than 0.4 m superimposed on the low-frequency wave heights. Previous studies indicate the wake amplitude is related to ship size and speed (Ng and Byres, 2011; Scarpa et al., 2019). However, observations at Pea Patch Island did not follow a discernable pattern when classified by length (Figure 7E) or average speed

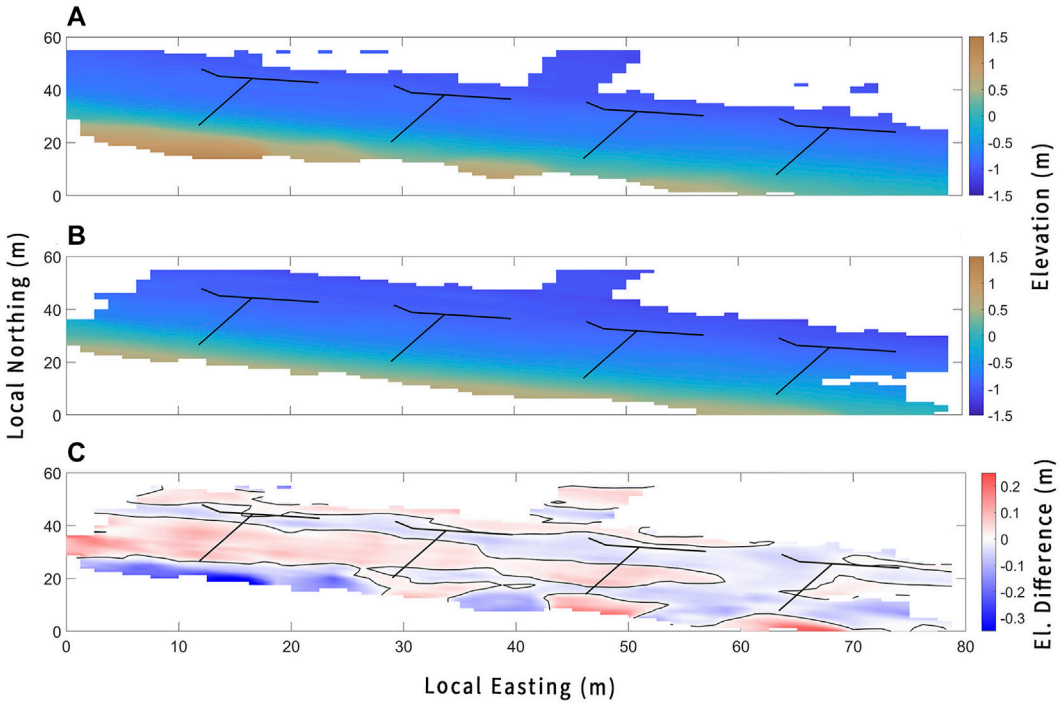


FIGURE 6
Elevation surveys taken in **(A)** May and **(B)** September and **(C)** the difference between the two surveys in **(A)** and **(B)**. THGs are delimited by black lines. In **(C)** the zero-contour line is shown in black.

(Figure 7F). Observed ship wake variation may result from tidal level, distance from sailing line to shore, or ship draft.

A notable difference was observed during northbound and southbound ship wake events. For northbound ship wakes, the orientation of the shoreline with respect to the orientation of the shipping channel creates a strong alongshore component of the wave train. The heads of the THGs were modified to impede the propagation of this alongshore wave train, as noted in Section 2.2. The distinct alongshore component of a northbound ship wake was not present in southbound wake events. As such, northbound and southbound ship wakes events were analyzed separately to examine whether the alongshore component had an effect on the efficiency of the installation.

Velocity data were collected for 52 ship wake events when the JFEs were active (see Section 2.3). Magnitudes of peak offshore ship wake velocities in the cross-shore direction reached ~0.5 m/s and magnitudes of time-averaged (over the 20-min window) offshore cross-shore ship wake velocities reached ~0.2 m/s. In the alongshore direction, magnitudes of peak ship wake velocities reached ~0.4 m/s, and magnitudes of time-averaged (over the 20-min window) alongshore ship wake velocities reached ~0.2 m/s. Ranges of peak northbound and southbound ship wake cross-shore and alongshore velocities are shown as gray lines in Figures 8A–D. Peak velocities of all ship wake events were averaged to obtain the peak velocities of a typical ship passing the site (delineated by circles in Figure 8) and 98% confidence interval (black lines in Figure 8), where solid markers/lines represent positive (offshore or north-directed) velocities and dotted lines/open markers represent negative (onshore or south-directed) velocities. Cross-shore velocities decayed as the waves propagated through the installation from the offshore (C4) to onshore (C1) station (Figures 8A,C). Over the range of ship wake events, the trend of cross-shore velocity decay through the installation is more obvious for northbound ship wake events. However, for southbound ship wake events, the decrease in cross-shore velocity between the offshore station (C4) and the start of the installation (C3) indicates an installation-induced cross-shore velocity decay. For the typical northbound ship wake event, the peak cross-shore velocity decreased from ~0.08 ± 0.03 m/s (98% confidence interval) at C4 to ~0.05 ± 0.02 m/s (98% confidence interval) at C1. For the typical southbound ship wake event, the peak cross-shore velocity decreased from ~0.08 ± 0.03 m/s (98% confidence interval) at C4 to ~0.07 ± 0.01 m/s (98% confidence interval) at C1. Regardless of ship wake presence or direction, the net alongshore current is northerly directed (Figures 8B,D). The presence of a north-directed alongshore velocity for a southbound ship or a south-

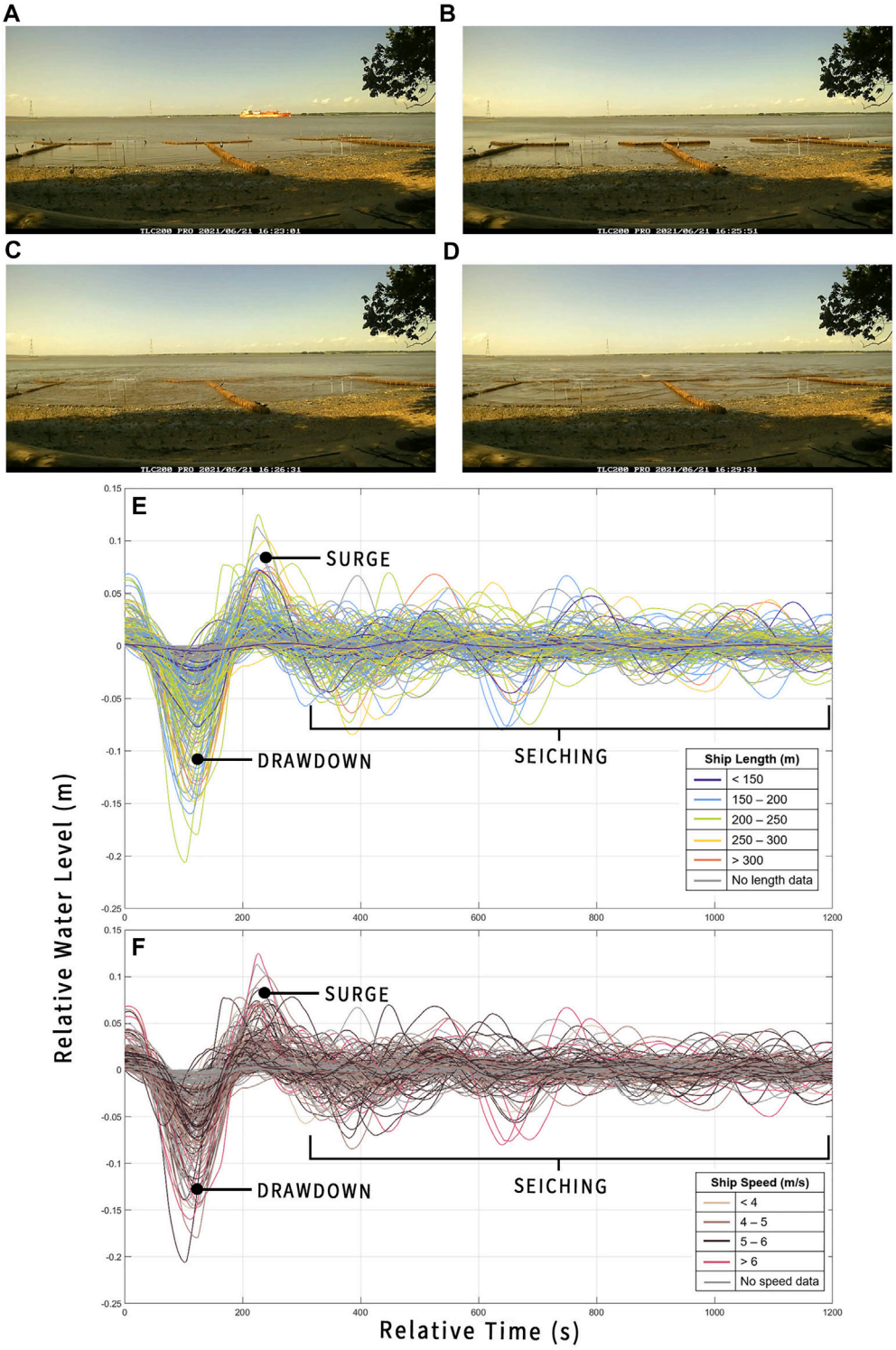


FIGURE 7
Snapshots of signature ship wake event structure: **(A)** elevated water level with ship path, **(B)** drawdown, **(C)** surge, and **(D)** high-frequency wave train. The low-frequency water level follows the graph of each event in **(E)** and **(F)** with notable features called out. Events are organized by ship length in **(E)** and average ship speed in **(F)**.

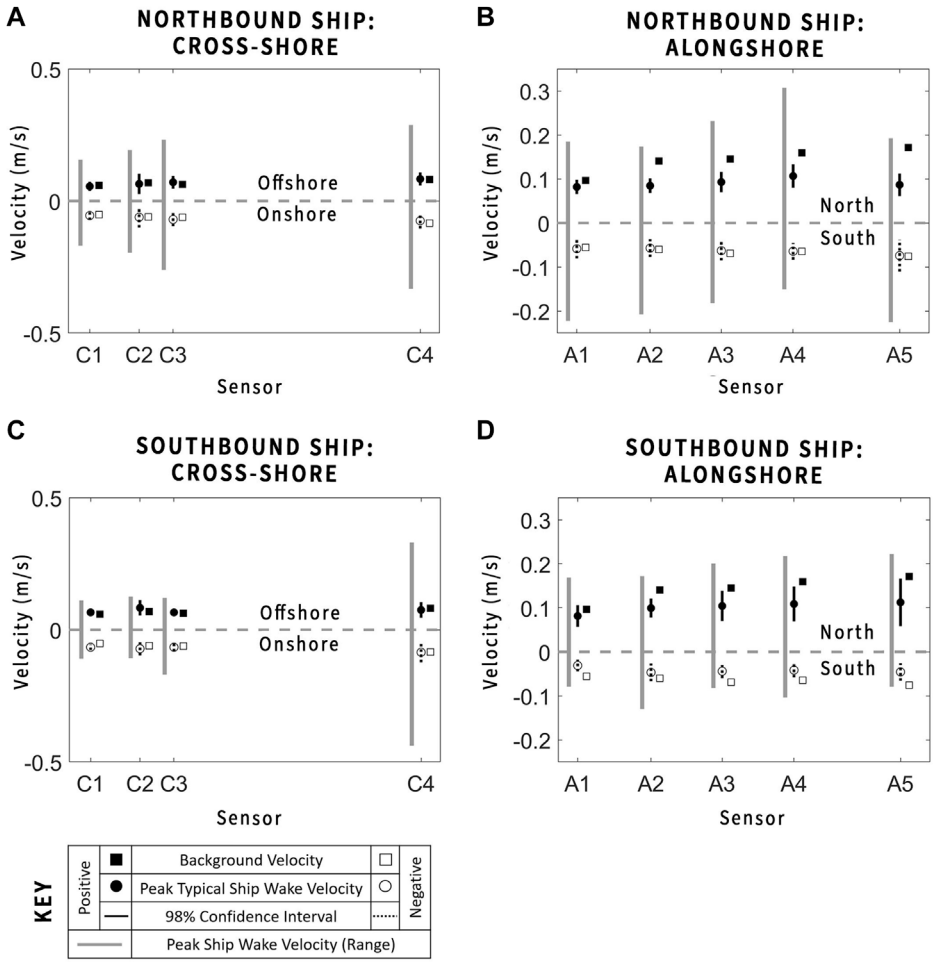


FIGURE 8
Peak (98th percentile) velocities in the cross-shore **(A,C)** and alongshore **(B,D)** directions for northbound **(A,B)** and southbound **(C,D)** ship wake events. Solid black lines/markers denote positive (offshore or north-directed) velocities and dotted lines/open markers denote negative (onshore or south-directed) velocities. Gray lines denote the ranges for ship wakes, black lines denote 98th percent confidence interval, circles are the ensemble-average for ship wakes, and squares are background conditions.

bound alongshore velocity for a northbound ship may be attributed to a dominant tidal current which exceeded the ship wake-induced alongshore current (Figure 8).

Velocity data were removed from the record for the 20-min period following all wake events (including those not analyzed) and the remaining data were taken as background conditions (represented by squares in Figure 8), which includes wind wave-induced velocities as well as tidal current velocities. Background conditions, unaffected by ship wake, are the same for the northbound and southbound ship wake event plots. Peak background velocities in the cross-shore (0.05–0.08 m/s) and alongshore (0.06–0.17 m/s) directions were, on average, ~74% and ~54% smaller, respectively, than the largest peak ship wake velocities (0.08–0.4 m/s; Figure 8). Peak background velocities are within ~10% of *typical* peak ship wake velocities (0.04–0.08 m/s; Figure 8). However, peak north-directed background velocities are ~51% greater than average peak north-directed ship wake velocities (0.08–0.1 m/s), indicating net flow in a northerly direction regardless of ship wake events at the site (Figures 8B,D).

## 3.3 Wave energy flux

Linear wave theory can be used to provide a rough estimate of energy dissipation through the installation. Changes in wave height, as opposed to other variables, are

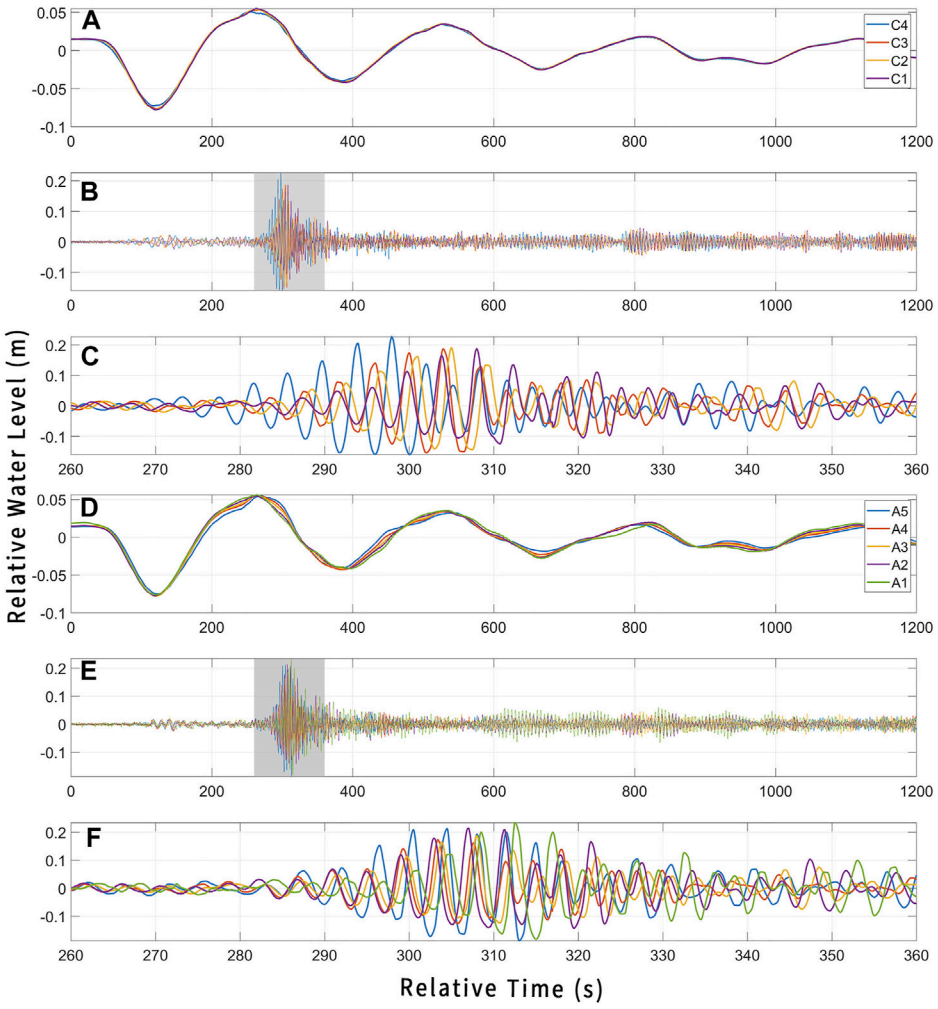


FIGURE 9
Propagation of a sample southbound wake event through the installation, where **(A–C)** show the cross-shore sensor array and **(D–F)** show the alongshore sensor array. **(A)** and **(D)** are the low-frequency signal; **(B)** and **(E)** are the high-frequency signal; and **(C)** and **(F)** are the high-frequency signal contained in the shaded area in **(B)** and **(E)**, respectively.

addressed first because the energy flux is a function of the wave height squared.

Water levels for sample southbound and northbound events are displayed in Figures 9, 10, respectively, where subplots A-C show the cross-shore component and subplots D-F show the alongshore component of the wake. In Figures 9, 10, subplots A and D show the low frequency (typical periods > 100 s) while subplots B and E show the high-frequency signal (typical period < 5 s) over the 20-min event duration. Subplots C and F show the same high-frequency signal over the time duration shaded in subplots B and E. Cross-shore sensors are denoted as C1–C4, onshore to offshore, and alongshore sensors are denoted as A1–A5, left to right (North to South), where C1 and A3 are the same station. Northbound wakes first reach C4 and A5, and southbound wakes first reach C4, lacking a significant alongshore wave component. It should be noted that the sample southbound event, which occurred on August 11, beginning at 13:09:43, represents some of the largest waves at the site over the course of the study, while the sample northbound event, which occurred on July 25, beginning at 9:22:17, had relatively small waves for a typical event at the site.

The installation tended to have a minimal impact on the low-frequency waves of the ship wake event (Figures 9A, 10A), but reduction of wave height is more significant for the high-frequency waves (Figures 9C, 10C) in the cross-shore direction. However, in the case of a northbound ship wake

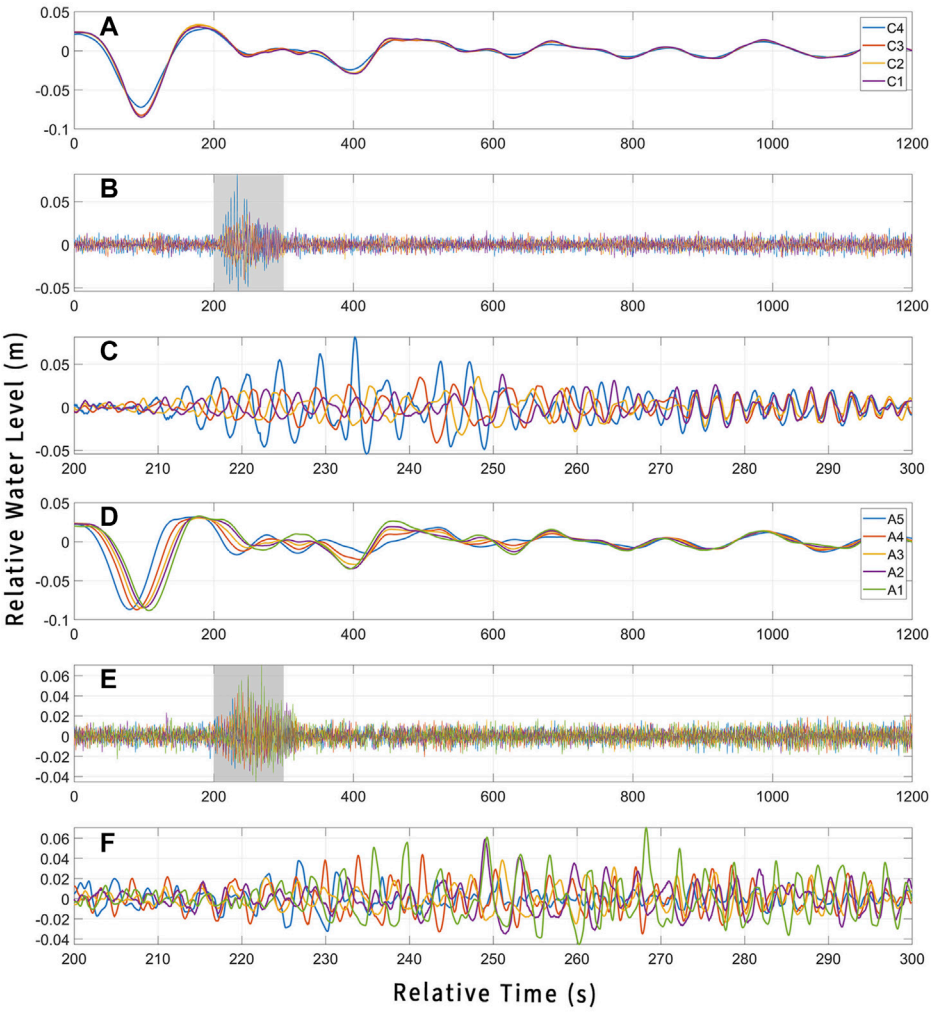


FIGURE 10
Propagation of a sample northbound wake event through the installation, where **(A–C)** show the cross-shore sensor array and **(D–F)** show the alongshore sensor array. **(A)** and **(D)** are the low frequency signal; **(B)** and **(E)** are the high-frequency signal; and **(C)** and **(F)** are the high-frequency signal contained in the shaded area in **(B)** and **(E)**, respectively.

event, the orientation of the shoreline with respect to the orientation of the shipping channel creates a strong alongshore component of the wave train. As expected, in the case of a northbound ship wake event, there was a time delay between arrival of the wake event at successive sensors (Figure 10D) due to the propagation of the alongshore waves through the installation. The time delay was not observed in the case of a southbound ship wake event (Figure 9D) due to the lack of a strong alongshore wave component. For a southbound ship wake event, the waves were approximately shore-normal, so the wave train reached the alongshore sensor array at approximately the same time. As in the case of the cross-shore signals, there was little effect of the installation on the wave height of the low-frequency alongshore portion of the wake event (Figures 9D, 10D). In contrast to the cross-shore signals, there is no discernable positive or negative effect of the installation on the high-frequency signal in the alongshore direction (Figures 9F, 10F).

The total ship wake energy flux for an event was calculated as a summation of energy fluxes for individual waves in the low- and high-frequency signals. Ship wake data were removed from the signal, and flux calculations were performed over the remainder of the signal to obtain background energy conditions. The collected ship wake energy fluxes were averaged per day and compared to the daily averaged background energy experienced across the cross-shore transect. The study area is impacted by 11,000–25,000 N/m of wave power per day, 2,700–12,000 N/

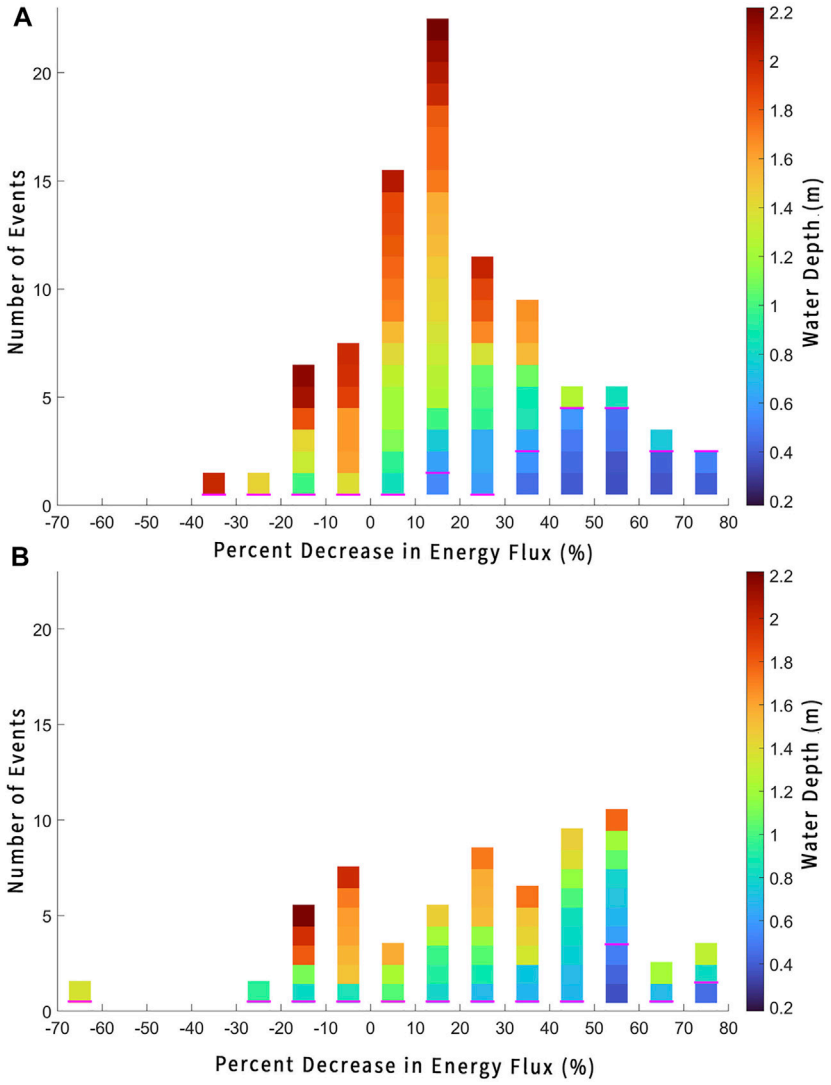


FIGURE 11
Histograms of percent decrease in energy flux from C4 to C1 for **(A)** southbound and **(B)** northbound ship wake events. Color represents water depth at sensor C4 for the event. Events above the magenta line take place with the heads of the THGs submerged.

m of which is ship wake-generated (depending on station and tidal level). Notably, ship wake events account for 25–50% of the energy flux impacting the area each day, but only account for roughly 22% of the duration of each day (~320 min). It is important to note that the overall energy flux imposed on the onshore regions of the beach was noticeably smaller than the offshore stations due to tidal influences resulting in varying water depth. The reduced exposure to natural hydrodynamic forces subsequently reduces the risk of ship-induced impacts.

Northbound and southbound ship wake events were analyzed separately to determine percent decrease in energy flux between C4 (offshore) and C1 (onshore). Decreases in energy flux were analyzed for trends over portions of the tidal cycle, and average ship speed, ship length, and water depth (Everett, Forthcoming 2022). Trends in the decrease in energy flux were most compelling in relation to water depth (Figure 11). The larger decreases in energy flux are represented by blue colors corresponding to shallower water depths. Similarly, in general, smaller decreases in energy flux (and amplifications of energy flux, see Section 4) are represented by red colors, corresponding to greater water depths. While the trend is more evident for southbound ship wake events, it is similar regardless of direction of ship travel. Events above the magenta line for each bin occurred when the heads of the THGs were submerged. Nineteen events (15 southbound and 4 northbound) occurred at shallower depths and had greater than a 10% decrease in

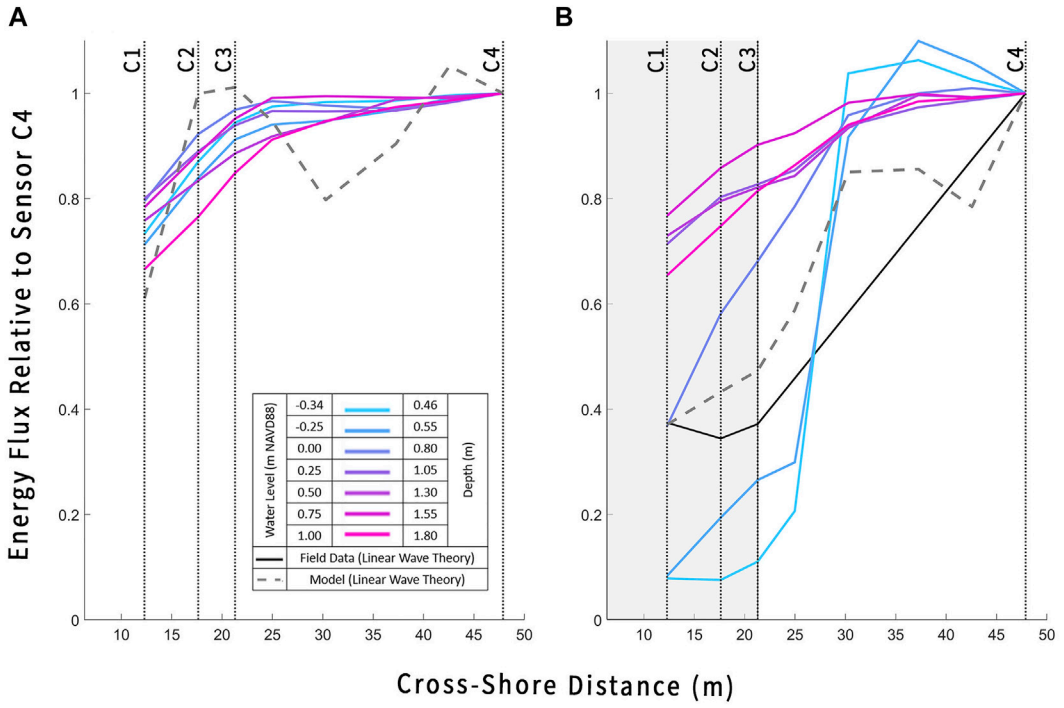


FIGURE 12
Modeled total energy flux normalized relative to C4 for simulations **(A)** with installation and **(B)** without installation. Dotted vertical lines denote labeled field sensor locations. Shaded area delineates the installation area.

energy flux and an average decrease in energy flux of ~50% (Figure 11).

Out of 87 southbound ship wake events, roughly a quarter had a decrease in energy flux between 10% and 20%. The distribution of percent decrease in energy flux is roughly Gaussian around this mean (Figure 11A). Nearly 11% of these events had greater than a 50% decrease in energy flux. The 60 northbound events do not have a similar distribution (Figure 11B). The largest bin of events (10) had a decrease of energy flux between 50% and 60%, larger than for the southbound events. However, these events represent only ~17% of the northbound wakes. Nearly a quarter of the northbound wakes had greater than a 50% decrease in energy flux.

## 3.4 Model Results

Energy dissipation has previously been shown to have a depth dependence for living shorelines designed to dissipate wave energy (Ellis et al., 2002; Chowdhury et al., 2019; Safak et al., 2020a). As such, FUNWAVE-TVD was used to simulate energy fluxes during wake conditions for water levels from −0.25 m to +1.0 m (NAVD88) at 0.25 m intervals, and the previously tested water level of −0.34 m. At water levels of approximately −0.4 m, the heads of the THGs are just submerged. JS INEOS INTUITION, a large oil tanker travelling northbound at ~7 m/s was used for the simulation. The length, width, and draft of the simulated vessel are 180, 26, and 6 m, respectively, where the draft was estimated through parameter studies (Williams, Forthcoming 2022).

Model simulations were performed first to estimate energy flux without the installation present. Depth-integrated energy flux, normalized to that at C4, was defined using the general definitions of kinetic and potential energy. Regardless of water level, the energy flux calculated at C1 was 60%–80% of the energy flux calculated at C4 (Figure 12A). An additional estimate was made for a water level of −0.34 m using linear wave theory with moderate comparison (10%–20% difference) to estimates based on kinetic and potential energy. Simulations with the THGs present (Figure 12B) show variation depending on water level. Linear wave theory estimates from the model (gray dashed line) and field data (solid black line) show similar trends but differences in the cross-shore decrease in energy flux. At C1, the energy flux decreases to ~40% of the energy flux at C4 and the linear wave theory estimates of energy flux are in good agreement. Modeled energy flux at C1 decreased to ~10% of the flux at C4 for −0.34 m and −0.25 m water levels (Figure 12B). At a water level of 0.0 m, the

energy flux at C1 was ~40% of the energy flux at C4, similar to the linear wave theory estimates at a water level of −0.34 m (Figure 12B). Reduction in energy flux to this extent did not occur for higher water level simulations, suggesting that the installation effectiveness decreases sharply between water levels of 0.0 and 0.25 m. For the highest water levels (0.75 and 1.0 m), indicative of high tides and storm surge, simulations with and without the THGs yielded similar results, indicating little to no installation-induced energy dissipation when the installation is submerged in a depth greater than 1.5 m. While estimates of energy flux using linear wave theory indicated that the installation is less effective when submerged, model results indicate that the installation may still be effective when submerged up to approximately twice its height. The simulations indicate that the installation could perform optimally for the lower 50% of the tidal range (up to 0.0 m NAVD88).

# 4 Discussion

Decreases in energy flux across the installation indicate a depth dependence in agreement with studies on oyster reefs (Taube, 2010; Chowdhury et al., 2019; Wiberg et al., 2019; Safak et al., 2020a), brush bundle breakwaters, (Ellis et al., 2002), coastal fringe marshes (Knutson et al., 1982), and laboratory studies (van der Meer et al., 2005) and numerical simulations (Ting et al., 2004) on porous breakwaters. Morris et al. (2018) note that there is likely an optimal depth for living shorelines, and at greater depths, there is a decoupling of the interaction between surface waves and the habitat or structure. Over the lower 25% of the tidal range (up to −0.4 m elevation), the full impact of the THG was expected to be realized and was supported by field observations. During the surge and successive waves, water would impinge the heads of the THGs, often filtering through the gaps between THGs and eventually overtopping the heads of the THGs. A clear diffraction pattern was visible when water moved through the gaps, indicating a potential for additional energy dissipation. The natural trenching extending onshore from the gaps between the heads of the THGs noted in similar living shorelines (Dinh et al., 2013) was absent at the Pea Patch Island study site. However, the sediment accumulation between comparable emergent THGs (Dinh et al., 2013) is similar to that behind the heads of the three western THGs on the Pea Patch Island site (Figure 6C). The accretion observed at the three western THGs was approximately twice the expected error in elevation measurements, indicating that the actual change in elevation may have been between 0.05 and 0.15 m.

Kraus et al. (1994) recommend that groins not be used in environments where overpassing may occur at high tides. When overpassing occurred at the present study site, the installation may behave akin to a submerged breakwater where wave attenuation of the structure deceases with increased depth of the crest of the structure (Dean et al., 1994). When the installation was submerged approximately twice its height (over ~50% of the tidal range), little to no effect on the energy flux was identified (Figure 12B), similar to oyster reefs (Wiberg et al., 2019) and segmented breakwaters (Dean et al., 1994). In fact, the greatest energy flux reduction occurred when the THGs were submerged between 50%–138% of their height, in agreement with the optimal water level range of ± 0.25 m of the crest of the structure reported by Wiberg et al. (2019). In addition, breakwaters submerged in depths 100%–125% of their height tend to display a specific circulation pattern dominated by a pumping mechanism rather than background alongshore currents (Dean et al., 1994). Water becomes trapped onshore of the structure and cannot form a typical undertow current. Rather, water travels as alongshore currents diverging from the center of the structure along the onshore side until it reaches a gap in the structure and forms a roughly shore normal offshore flowing current (Dean et al., 1994). The alongshore current generated by the pumping mechanism can be up to five times as strong as the undertow current in a control condition (Dean et al., 1994), which can cause increased sediment motion and potential erosion onshore of the structure. This circulation pattern, observed during lower tide levels and wakes from southbound ships, is a likely explanation for the small-scale erosion evident onshore of the heads of the THGs (Figure 6C).

The structure-induced flow alteration can lead to enhanced sediment motion. Critical bottom shear stresses, $\tau_{b,cr}$, for fine-grained sediment on a similar tidal flat ranged from 0.10 to 2.0 N/m$^2$ (Lanuru, 2008). Bottom shear stress can be estimated through the quadratic drag law as

$$\tau_b = \frac{1}{2}\rho f u^2 \tag{4}$$

where $u$ is the magnitude of the instantaneous velocity and $f$ is a friction factor. Friction factors depend on Reynolds number and grain characteristics and can vary widely. A friction factor of 0.05 is used here (Lacy and MacVean, 2016). Inverting Eq. (4) provides a range of critical velocities $u_{cr}$ for motion of fine-grained sediment as

$$u_{cr} = \sqrt{\frac{2\tau_{b,cr}}{\rho f}} = 0.06 - \ 0.3\text{m/s} \tag{5}$$

Near bed velocities were not collected behind the heads of the THGs. However, near bed velocities at C3, between the heads of the THGs, indicate, based on this simple analysis, that critical velocities for sediment motion are exceeded under ship wake conditions over 50% of the time. These simple estimates are supported by visual observation of turbid water during ship wake events near the heads of the THGs during low tides.

In the case of obliquely incident waves, the interaction of the alongshore current with pumping-induced return flow can lead to accretion on the downdrift end of the structure (Ranasinghe and Turner, 2006). Northbound wakes, due to

the orientation of the channel and shoreline, produced obliquely incident waves at the study site. The increased accretion on the downdrift (western) end of the installation as compared to the updrift (eastern) end indicates the dominance of northbound ship wake activity in combination with a net north-directed flow (flood dominance) at the site. Notably, higher overall energy dissipation occurred for northbound ship wake events. The greater effect by the structure on the northbound ship wakes is further supported by the decay of the alongshore current down-drift of the eastern THG. Further understanding of the circulation patterns within the installation would require additional investigation and more spatially resolved velocity data.

Interestingly, in both directions of ship wake propagation, there are outliers with an *increase* in energy flux (Figure 11). All increases in energy flux occurred when the installation was fully submerged, which may indicate wave reflection and constructive convergence due to limited offshore wave breaking in deeper water. Amplification of energy flux may be attributed to sensor noise and the assumption of linear wave theory for events with an increase of energy flux up to 10%. For the remaining 15 events, many of which occurred at night, timelapse footage was analyzed, but no discernable disturbance or anomaly was detected. It may be suggested that, for the northbound ship wake events, the shore normal wave train may converge with the alongshore wave train from the south, leading to wave amplification. For southbound ship wake events, there may be some impact of the sand shoals north of the site. Limitations imposed by the experimental layout prevent further investigation.

Further analysis of the effect of the installation on the erosional trend of the northeastern beach on Pea Patch Island would require long-term monitoring of the project. One way to predict potential performance of this living shoreline is to examine the performance over approximately two years of a similarly shaped living shoreline (Albers and Schmitt, 2015). Those structures were able to reduce wave heights up to 80% and performed most effectively when not submerged (Albers and Schmitt, 2015). Additionally, structure-induced sedimentation with similar sediment characteristics as the Pea Patch Island tidal flat allowed floodplain and mangrove forest recovery (Albers and Schmitt, 2015). Notably, the Albers and Schmitt (2015) study reported shorter period higher amplitude waves, and a larger tidal range, than the ship wake forcing studied at Pea Patch Island. As such, the Pea Patch Island wave climate may be less energetic than that studied by Albers and Schmitt (2015), making it a potentially more suitable environment for the success of a living shoreline installation in the absence of storm conditions. Although living shorelines are site specific, it is expected that the general morphological changes (erosion and accretion patterns on the tidal flat) observed at Pea Patch Island could have continued if calm and ship-wake conditions remained similar to those during the study period.

Guidance for the design and use of living shorelines in different environments and under different conditions is still being developed. Most guidance recommends soft solutions (no hard structural component such as rock) only be used in low energy environments, which is typically described as waves heights < 0.3 m or minimal wave and boat action (NOAA, 2015; Miller et al., 2016; Delaware Living Shorelines Committee, 2020). Ship wakes can increase the energy level of the wave climate at a site (Hardaway et al., 2017); at Pea Patch Island, maximum ship wake heights are more typical of an environment with moderate energy levels (wave heights 0.3–0.6 m). In addition, previous reports have indicated that coir logs are not a recommended material for high energy saltwater environments or environments with significant boating activity (Duhring, 2008; Skrabal, 2013). Often when design guidelines refer to wake, the relation is to smaller, recreational boats rather than large container ships and tankers. Despite this prior guidance, results from Pea Patch Island indicate that coir logs arranged in a repeating T-head groin configuration may offer some wave attenuation and erosion protection to a silty-mud tidal flat affected by ship wake energy. However, the installation was not robust under storm conditions. Storms may increase in frequency and severity during winter months when *in situ* data were not available. Review of timelapse footage during the winter season indicated structural failure, coir log damage, and coir log shiftings. As such, it is likely that the installation would not be effective year-round. Thus, a coir log installation may not be suitable under sustained high energy conditions, but may be effective in mitigating intermittent moderate energy activity induced by ship wakes similar to conditions at Pea Patch Island (when storm energy is not a factor). A different design approach, potentially a hybrid solution including some hard features, may be necessary for an effective mitigation scheme at this site and similar sites affected by ship wake forcing and seasonal storms.

## 5 Conclusion

Results of this investigation indicate the severity of negative outcomes arising from ship wakes reaching the shores of the Delaware River Estuary as well as the ability of living shoreline configuration made up of coir log T-head groins to mitigate the effects of ship wakes.

1) Ship wakes account for 25–50% of the total daily energy impacting the shoreline at the site. Peak background velocities are, on average, ~74% (~54%) smaller than the largest cross-shore (alongshore) ship wake velocities. In a moderate fetch confined compound channel, ship wakes can contribute a considerable amount of energy to the hydrodynamic system and increase nearshore velocities.

2) Northbound and southbound ship wake events had different outcomes in part due to the alongshore component of northbound ship wakes. Approximately 11% of southbound wake events had a decrease in energy flux greater than 50% whereas ~25% of northbound ship wake events displayed a similar decrease in energy flux. Channel and nearshore bathymetry play a significant role in the transformation of ship wakes from offshore to onshore, which has implications for the performance of any structure intended to decrease the total energy impacting the shoreline.
3) The installation displayed a strong depth dependence. Over the lower 25% of the tidal range, the installation induced a wave diffraction pattern between the THGs that resulted in onshore accretion of up to 0.1 m and decreases in energy flux of 10–80%. The installation had potential to reduce wave energy impacting the shoreline over the lower 50% of the tidal range and when submerged up to twice its height. The tidal range at a given site and placement of shoreline protection implements within that range are important variables in the performance and efficacy of a living shoreline installation.
4) Morphological changes are commensurate with observations near submerged breakwaters under oblique wave forcing. Erosion of up to 0.1 m occurred just onshore of the heads of the THGs, likely due to the circulation pattern created by a structure-induced pumping mechanism. Shoreline changes showed a larger area of accretion of up to 0.1 m on the northern side of the installation likely due to the interaction of the circulation pattern and north-directed alongshore current. Elevation changes of up to 0.2 m were observed onshore of the installation area. A natural low-crested breakwater arranged in a THG configuration on an estuarine shoreline can produce circulation patterns and morphological changes comparable to similarly designed hard shoreline protection measures.
5) Coir logs were sustained and secured in place through ship wake, non-storm conditions but were damaged during storm conditions. Monitoring of the installation with the time-lapse footage revealed the dislodging and loss of coir logs from their original position. Coir logs demonstrate an ability to sustain position through ship wake conditions in areas with moderate fetch, allowing accretion to occur. However, coir logs may not be suitable for long-term installations addressing ship wake in moderate fetch areas where increased energy from storms is a factor.

Though living shorelines are generally only recommended for low energy environments, results indicate the potential application of nature-based solutions (including coir logs) in environments with intermittent higher energy activity produced by large vessel shipping traffic. Future research directions may investigate alternate nature-based materials and designs in areas affected by ship wakes, or potential hybrid approaches to address storm events in areas with a similar moderate fetch.

## Data availability statement

The raw data supporting the conclusion of this article will be made available by the authors, without undue reservation.

## Author contributions

CE: original draft preparation, field data collection and analysis, figure generation, manuscript editing, manuscript preparation; OW: original draft preparation (numerical simulation sections), field data collection, model domain update, model validation, numerical simulation analysis, figure generation; ER: original draft preparation, living shoreline design preparation, figure preparation and formatting; ML: original draft contributions, figure generation, manuscript review; RS: original draft contributions, manuscript review; MM: manuscript review; FS: project conceptualization, funding acquisition, manuscript review; JB: project conceptualization, funding acquisition, project administration and supervision, permit acquisition; JP: project conceptualization, funding acquisition, project administration and supervision, manuscript editing.

## Funding

This work was supported by Delaware Sea Grant (NA18OAR4170086) and the University of Delaware.

## Acknowledgments

The authors gratefully acknowledge the support of individuals affiliated with the Center for Applied Coastal Research and Coastal Resilience Design Studio for their help in the construction and monitoring of the living shoreline, including Olivia Amante, Erica Beddings, David Bogart, Conner Brown, Nick Bruce, Emily Chapman, Delaney Doran, Maya Eley, Seth Esterly, William Everett, Christopher Fettke von Koeckritz, Heather Fettke von Koeckritz, Andrew Gainey, Joshua Gainey, Manoj Kumar Gangadharan, Mackenzie Hammel, Ben Horney, Temitope Ezekiel Idowu, Evan Mazur, Mohammad Sadegh Nouri, Courtney Olney, Maria Pontiki, Kyle Rumaker, Martha Ryan and Mike Welsh. The authors express the utmost gratitude to John Mercer, Linton Mercer, and Kingfisher Environmental Services, Inc. for providing in-kind services. The authors acknowledge the work of Taira Baldauf in data analysis for pilot studies in conjunction with this investigation. The authors additionally thank the Delaware Department of Natural Resources and Environmental Control (DNREC) for providing site

access, transportation, and assistance in initial site location determination. We appreciate the critical reviews that improved clarity of the manuscript. Portions of this work were utilized and acknowledged in a master's thesis for both Cassandra Everett and Oscar Williams.

## Conflict of interest

ML was employed by Sustainable Coastal Solutions, Inc.

The remaining authors declare that the research was conducted in the absence of any commercial or financial relationships that could be construed as a potential conflict of interest.

## Publisher's note



## References

Albers, T., and Schmitt, K. (2015). Dyke design, floodplain restoration and mangrove co-management as parts of an area coastal protection strategy for the mud coasts of the Mekong Delta, Vietnam. *Wetl. Ecol. Manag.* 23 (6), 991–1004. doi:10.1007/s11273-015-9441-3

Almaz, O., and Altiok, T. (2012). Simulation modeling of the vessel traffic in Delaware River: impact of deepening on port performance. *Simul. Model. Pract. Theory* 22, 146–165. doi:10.1016/j.simpat.2011.12.004

Baldauf, T. (2021). *Quantifying the effect of ship wake on commonly used living shoreline treatments*. undergraduate thesis. Newark (DE): University of Delaware.

Bayraktarov, E., Stewart-Sinclair, P. J., Brisbane, S., Boström-Einarsson, L., Saunders, M. I., Lovelock, C. E., et al. (2019). Motivations, success, and cost of coral reef restoration. *Restor. Ecol.* 27 (5), 981–991. doi:10.1111/rec.12977

Bilkovic, D., Mitchell, M., Davis, J., Herman, J., Andrews, E., King, A., et al. (2019). Defining boat wake impacts on shoreline stability toward management and policy solutions. *Ocean Coast. Manag.* 182, 104945. doi:10.1016/j.ocecoaman.2019.104945

Brophy, L., Greene, C., Hare, V., Holycross, B., Lanier, A., Heady, W., et al. (2019). Insights into estuary habitat loss in the Western United States using a new method for mapping maximum extent of tidal wetlands. *PLOS ONE* 14 (8), e0218558. doi:10.1371/journal.pone.0218558

Chowdhury, M. S. N., Walles, B., Sharifuzzaman, S., Shahadat Hossain, M., Ysebaert, T., Smaal, A. C., et al. (2019). Oyster breakwater reefs promote adjacent mudflat stability and salt marsh growth in a monsoon dominated subtropical coast. *Sci. Rep.* 9, 8549. doi:10.1038/s41598-019-44925-6

Cook, T., Sommerfield, C., and Wong, K. (2007). Observations of tidal and springtime sediment transport in the upper Delaware Estuary. *Estuar. Coast. Shelf Sci.* 72 (1-2), 235–246. doi:10.1016/j.ecss.2006.10.014

Dao, T., Stive, M. J. F., Hofland, B., and Mai, T. (2018). Wave damping due to wooden fences along mangrove coasts. *J. Coast. Res.* 34 (6), 1317. doi:10.2112/jcoastres-d-18-00015.1

Davis, J. L., Currin, C. A., O'Brien, C., Raffenburg, C., and Davis, A. (2015). Living shorelines: coastal resilience with a blue carbon benefit. *PLOS ONE* 10, e0142595. doi:10.1371/journal.pone.0142595

De Roo, S., and Troch, P. (2015). Evaluation of the effectiveness of a living shoreline in a confined, non-tidal waterway subject to heavy shipping traffic. *River Res. Appl.* 31 (8), 1028–1039. doi:10.1002/rra.2790

Dean, R., and Dalrymple, R. (2002). *Coastal processes with engineering applications*. Cambridge: Cambridge University Press.

Dean, R. G., Browder, A. E., Goodrich, M. S., and Donaldson, D. G. (1994). *Model tests of the proposed P.E.P. Reef installation at Vero Beach, Florida*. Gainesville: Coastal and Oceanographic Engineering Department, University of Florida. UFL/COEL-94-012FL28 pp. plus 2 appendices. [online] Available at: https://ufdc.ufl.edu/UF00085003/00001 (accessed January 12, 2022).

Delaware Department of Natural Resources and Environmental Control (DNREC) (2020). *SAA for tidal and non-tidal shoreline stabilization*. [online] Available at: http://www.dnrec.delaware.gov/wr/Documents/Shoreline_Stabilization_SAA.pdf (accessed May 20, 2022).

Delaware Department of Natural Resources and Environmental Control (DNREC) (2001). "The Pea Patch island heronry region special management plan. Progress report," in *Three years of strategy implementation*.

Delaware Living Shorelines Committee (2020). *Site evaluation for living shoreline projects in Delaware*. [online] Available at: https://static1.squarespace.com/static/59b69f4f2994caee6bf52abe/t/5ea82bf97189b11145040d10/1588079656882/DelawareLivingShorelineSiteEvaluation_v10.pdf (accessed January 12, 2022).

Dinh, S., Albers, T., and Schmitt, K. (2013). "Shoreline management guidelines coastal protection in the lower mekong delta," in *Deutsche Gesellschaft für Internationale Zusammenarbeit (GIZ) GmbH*.

Douglass, S. L., and Pickel, B. H. (1999). The tide doesn't go out anymore: the effect of bulkheads on urban bay shorelines. *Shore Beach* 67 (2-3), 19–25. [online] Available at: https://www.mobilebaynep.com/assets/pdf/Effect_of_Bulkheads_on_Urban_Shorelines.pdf (accessed January 12, 2022).

Duhring, K. A. (2008). *A comparison of structural and nonstructural methods for erosion control and providing habitat in Virginia salt marshes proceedings of the 2006 living shoreline summit (Williamsburg, Virginia)*. Gloucester Point, Virginia: Coastal Resources Commission CRC, 41–47. Publication No. 08-164.

Ellis, J., Sherman, D., Bauer, B., and Hart, J. (2002). Assessing the impact of an organic restoration structure on boat wake energy. *J. Coast. Res.* 36, 256–265. doi:10.2112/1551-5036-36.sp1.256

Everett, C. (Forthcoming 2022). *Performance of a living shoreline under ship wake forcing on an estuarine shoreline*. master's thesis. Newark (DE): University of Delaware.

Ezcurra, E., Barrios, E., Ezcurra, P., Ezcurra, A., Vanderplank, S., Vidal, O., et al. (2019). A natural experiment reveals the impact of hydroelectric dams on the estuaries of tropical rivers. *Sci. Adv.* 5 (3), eaau9875. doi:10.1126/sciadv.aau9875

Forlini, C., Qayyum, R., Malej, M., Lam, M., Shi, F., Angelini, C., et al. (2021). On the problem of modeling the boat wake climate: the florida intracoastal waterway. *J. Geophys. Res. Oceans* 126 (2). doi:10.1029/2020jc016676

Gabel, F., Lorenz, S., and Stoll, S. (2017). Effects of ship-induced waves on aquatic ecosystems. *Sci. Total Environ.* 601-602, 926–939. doi:10.1016/j.scitotenv.2017.05.206

Gedan, K., Kirwan, M., Wolanski, E., Barbier, E., and Silliman, B. (2011). The present and future role of coastal wetland vegetation in protecting shorelines: Answering recent challenges to the paradigm. *Clim. Change* 106 (1), 7–29. doi:10.1007/s10584-010-0003-7

Gharbi, S., Hamdi, G., Valkov, G., and Nistor, I. (2008). *Field measurements of ship waves along the St. Lawrence river waterway*. Canada, 1–10. OCEANS 2008. doi:10.1109/OCEANS.2008.5152138

Gittman, R., Fodrie, F., Popowich, A., Keller, D., Bruno, J., Currin, C., et al. (2015). Engineering away our natural defenses: an analysis of shoreline hardening in the US. *Front. Ecol. Environ.* 13 (6), 301–307. doi:10.1890/150065

Gittman, R., Popowich, A., Bruno, J., and Peterson, C. (2014). Marshes with and without sills protect estuarine shorelines from erosion better than bulkheads during a category 1 hurricane. *Ocean Coast. Manag.* 102, 94–102. doi:10.1016/j.ocecoaman.2014.09.016

Gourlay, T. (2001). The supercritical bore produced by a high-speed ship in a channel. *J. Fluid Mech.* 434, 399–409. doi:10.1017/s002211200100372x

Hardaway, C. S., Jr., Milligan, D. A., Duhring, K., and Wilcox, C. A. (2017). *Living shoreline design guidelines for shore protection in virginia's estuarine environment (SRAMSOE #463)*. Gloucester Point, VA: Virginia Institute of Marine Science. doi:10.21220/V5CF1N

Herbert, D., Astrom, E., Bersoza, A., Batzer, A., McGovern, P., Angelini, C., et al. (2018). Mitigating erosional effects induced by boat wakes with living shorelines. *Sustainability* 10 (2), 436. doi:10.3390/su10020436

Houser, C. (2011). Sediment resuspension by vessel-generated waves along the savannah river, Georgia. *J. Waterw. Port. Coast. Ocean. Eng.* 137 (5), 246–257. doi:10.1061/(asce)ww.1943-5460.0000088

Kamphuis, J. W. (2010). Introduction to coastal engineering and management: 2nd edition. *Adv. Ser. Ocean Eng.* 30, 1–564. doi:10.1142/9789812834867_0001

Kibler, K. M., Kitsikoudis, V., Donnelly, M., Spiering, D. W., and Walter, L. (2019). Flow-vegetation interaction in a living shoreline restoration and potential effect to mangrove recruitment. *Sustainability* 11 (11), 3215. doi:10.3390/su11113215

Knutson, P., Brochu, R., Seelig, W., and Inskeep, M. (1982). Wave damping in *Spartina alterniflora* marshes. *Wetlands* 2 (1), 87–104. doi:10.1007/bf03160548

Komar, P. (1998). *Beach processes and sedimentation*. Upper Saddle River (New Jersey): Prentice-Hall.

Kraus, N. C., Hanson, H., and Bomgren, H. S. (1994). "Modern functional design of groin systems," in *Proceedings ICCE 1994*, 1327–1342.

Lacy, J., and MacVean, L. (2016). Wave attenuation in the shallows of san francisco bay. *Coast. Eng.* 114, 159–168. doi:10.1016/j.coastaleng.2016.03.008

Lanuru, M. (2008). Measuring critical erosion shear stress of intertidal sediments with eromes erosion device. *Fak. Ilmu Kelaut. Dan. Perikan. Unhas* 18 (5), 390–397.

Mai Van, C., Ngo, A., Mai, T., and Dao, H. (2021). Bamboo fences as a nature-based measure for coastal wetland protection in Vietnam. *Front. Mar. Sci.* 8. doi:10.3389/fmars.2021.756597

Marani, M., d'Alpaos, A., Lanzoni, S., and Santalucia, M. (2011). Understanding and predicting wave erosion of marsh edges. *Geophys. Res. Lett.* 38 (21). doi:10.1029/2011gl048995

Meyer, D., Townsend, E., and Thayer, G. (1997). Stabilization and erosion control value of oyster cultch for intertidal marsh. *Restor. Ecol.* 5 (1), 93–99. doi:10.1046/j.1526-100x.1997.09710.x

Miller, J., Rella, A., Williams, A., and Sproule, E. (2016). *Living shorelines engineering guidelines*. SIT-DL-14-9-2942. [online] Available at: https://www.nj.gov/dep/cmp/docs/living-shorelines-engineering-guidelines-final.pdf (accessed January 12, 2022).

Millero, F., and Poisson, A. (1981). International one-atmosphere equation of state of seawater. *Deep Sea Res. Part A. Oceanogr. Res. Pap.* 28 (6), 625–629. doi:10.1016/0198-0149(81)90122-9

Morris, R., Konlechner, T., Ghisalberti, M., and Swearer, S. (2018). From grey to green: Efficacy of eco-engineering solutions for nature-based coastal defence. *Glob. Chang. Biol.* 24 (5), 1827–1842. doi:10.1111/gcb.14063

Neumann, B., Vafeidis, A., Zimmermann, J., and Nicholls, R. (2015). Future coastal population growth and exposure to sea-level rise and coastal flooding – a global assessment. *PLOS ONE* 10 (3), e0118571. doi:10.1371/journal.pone.0118571

Ng, M., and Byres, R. (2011). *Vessel wake study prepared for: KM LNG operating general partnership (M&N project No. 7333)*. Vancouver, BC: Moffat & Nichol. [online] Available at: https://docs2.cer-rec.gc.ca/ll-eng/llisapi.dll/fetch/2000/90466/94153/552726/657379/657474/670503/686250/B11-7-_2011.05.05.RPT.Vessel.Wake.Study_-_A1Z0S9_.pdf?nodeid=686399&vernum=-2 (accessed May 20, 2022).

NOAA (2015). Guidance for considering the use of living shorelines. [online] Available at: https://www.habitatblueprint.noaa.gov/wp-content/uploads/2018/01/NOAA-Guidance-for-Considering-the-Use-of-Living-Shorelines_2015.pdf (accessed January 12, 2022).

O'Donnell, J. (2017). Living shorelines: A review of literature relevant to new england coasts. *J. Coast. Res.* 332, 435–451. doi:10.2112/jcoastres-d-15-00184.1

Partnership for the Delaware Estuary (PDE) (2012). *Technical report for the Delaware estuary and basin*. PDF Report No. 12-01. 255 pages. [online] Available at: https://www.delawareestuary.org/science_programs_state_of_the_estuary.asp (accessed January 12, 2022).

Plant, N. G., Holland, K. T., and Puleo, J. A. (2002). Analysis of the scale of errors in nearshore bathymetric data. *Mar. Geol.* 191 (1-2), 71–86. doi:10.1016/S0025-3227(02)00497-8

Polk, M., and Eulie, D. (2018). Effectiveness of living shorelines as an erosion control method in North Carolina. *Estuaries Coasts* 41 (8), 2212–2222. doi:10.1007/s12237-018-0439-y

Proudman, J. (1963). *Dynamical oceanography*. London: Methuen.

Ralston, D., Talke, S., Geyer, W., Al-Zubaidi, H., and Sommerfield, C. (2019). Bigger tides, less flooding: effects of dredging on barotropic dynamics in a highly modified estuary. *J. Geophys. Res. Oceans* 124 (1), 196–211. doi:10.1029/2018jc014313

Ranasinghe, R., and Turner, I. (2006). Shoreline response to submerged structures: a review. *Coast. Eng.* 53 (1), 65–79. doi:10.1016/j.coastaleng.2005.08.003

Rapaglia, J., Zaggia, L., Parnell, K., Lorenzetti, G., and Vafeidis, A. (2015). Ship-wake induced sediment remobilization: effects and proposed management strategies for the Venice Lagoon. *Ocean Coast. Manag.* 110, 1–11. doi:10.1016/j.ocecoaman.2015.03.002

Ross, A., Najjar, R., Li, M., Lee, S., Zhang, F., Liu, W., et al. (2017). Fingerprints of sea level rise on changing tides in the chesapeake and Delaware bays. *J. Geophys. Res. Oceans* 122 (10), 8102–8125. doi:10.1002/2017jc012887

Safak, I., Angelini, C., Norby, P., Dix, N., Roddenberry, A., Herbert, D., et al. (2020a). Wave transmission through living shoreline breakwalls. *Cont. Shelf Res.* 211, 104268. doi:10.1016/j.csr.2020.104268

Safak, I., Angelini, C., and Sheremet, A. (2021). Boat wake effects on sediment transport in intertidal waterways. *Cont. Shelf Res.* 222, 104422. doi:10.1016/j.csr.2021.104422

Safak, I., Norby, P., Dix, N., Grizzle, R., Southwell, M., Veenstra, J., et al. (2020b). Coupling breakwalls with oyster restoration structures enhances living shoreline performance along energetic shorelines. *Ecol. Eng.* 158, 106071. doi:10.1016/j.ecoleng.2020.106071

SAGE (2015). *Natural and structural measures for shoreline stabilization*. [online] Available at: http://www.sagecoast.org/docs/SAGE_LivingShorelineBrochure_Print.pdf (accessed January 12, 2022).

Scarpa, G., Zaggia, L., Manfè, G., Lorenzetti, G., Parnell, K., Soomere, T., et al. (2019). The effects of ship wakes in the venice lagoon and implications for the sustainability of shipping in coastal waters. *Sci. Rep.* 9 (1), 19014. doi:10.1038/s41598-019-55238-z

Schaefer, R. (2019). *Impacts and vegetation-induced attenuation of wind- and vessel-generated waves*. undergraduate thesis. Newark (DE): University of Delaware.

Schroevers, M., Huisman, B., van der Wal, M., and Terwindt, J. (2011). in *2011 IEEE/OES 10th current, waves and turbulence measurements (CWTM)*. doi:10.1109/CWTM.2011.5759539*Measuring ship induced waves and currents on a tidal flat in the Western Scheldt estuary*

Shi, F., Malej, M., Smith, J., and Kirby, J. (2018). Breaking of ship bores in a boussinesq-type ship-wake model. *Coast. Eng.* 132, 1–12. doi:10.1016/j.coastaleng.2017.11.002

Skrabal, T. (2013). "Living shoreline projects in North Carolina," in *Proceedings of the 2013 mid-atlantic living shorelines summit* (Cambridge, Maryland), 29–30.

Smith, C., Gittman, R., Neylan, I., Scyphers, S., Morton, J., Joel Fodrie, F., et al. (2017). Hurricane damage along natural and hardened estuarine shorelines: using homeowner experiences to promote nature-based coastal protection. *Mar. Policy* 81, 350–358. doi:10.1016/j.marpol.2017.04.013

Smith, C., Rudd, M., Gittman, R., Melvin, E., Patterson, V., Renzi, J., et al. (2020). Coming to terms with living shorelines: a scoping review of novel restoration strategies for shoreline protection. *Front. Mar. Sci.* 7. doi:10.3389/fmars.2020.00434

Soomere, T. (2006). Nonlinear ship wake waves as a model of rogue waves and a source of danger to the coastal environment: a review. *Oceanologia* 48 (S), 185–202.

Soomere, T., Parnell, K. E., and Didenkulova, I. (2009). Implications of fast-ferry wakes for semi-sheltered beaches: a case study at aegna island, baltic sea. *J. Coast. Res.* 56 (1), 128–132.

Spencer, T., Schuerch, M., Nicholls, R. J., Hinkel, J., Lincke, D., Vafeidis, A. T., et al. (2016). Global coastal wetland change under sea-level rise and related stresses: the DIVa wetland change model. *Glob. Planet. Change* 139, 15–30. doi:10.1016/j.gloplacha.2015.12.018

Styles, R., and Hartman, M. (2019). Effect of tidal stage on sediment concentrations and turbulence by vessel wake in a coastal plain saltmarsh. *J. Mar. Sci. Eng.* 7 (6), 192. doi:10.3390/jmse7060192

Syvitski, J., Vörösmarty, C., Kettner, A., and Green, P. (2005). Impact of humans on the flux of terrestrial sediment to the global coastal ocean. *Science* 308 (5720), 376–380. doi:10.1126/science.1109454

Tait, J., and Griggs, G. (1991). *Beach response to the presence of a seawall; comparison of field observations*. Washington, DC: US Army Corps of Engineers.

Taube, S. R. (2010). *Impacts of fringing oyster reefs on wave attenuation and marsh erosion rates*. undergraduate thesis. Charlottesville (VA): University of Virginia.

Temmerman, S., Meire, P., Bouma, T., Herman, P., Ysebaert, T., De Vriend, H., et al. (2013). Ecosystem-based coastal defence in the face of global change. *Nature* 504 (7478), 79–83. doi:10.1038/nature12859

Ting, C., Lin, M., and Cheng, C. (2004). Porosity effects on non-breaking surface waves over permeable submerged breakwaters. *Coast. Eng.* 50 (4), 213–224. doi:10.1016/j.coastaleng.2003.10.003

USACE (2009). Delaware River main stem and channel deepening project environmental assessment. [online] Available at: https://www.nap.usace.army.mil/Portals/39/docs/Civil/Deepening/Environmental/Environmental%20Assessment%20-%20April%202009.pdf (accessed January 12, 2022).

van der Meer, J., Briganti, R., Zanuttigh, B., and Wang, B. (2005). Wave transmission and reflection at low-crested structures: Design formulae, oblique wave attack and spectral change. *Coast. Eng.* 52 (10-11), 915–929. doi:10.1016/j.coastaleng.2005.09.005

van Maren, D., van Kessel, T., Cronin, K., and Sittoni, L. (2015). The impact of channel deepening and dredging on estuarine sediment concentration. *Cont. Shelf Res.* 95, 1–14. doi:10.1016/j.csr.2014.12.010

van Rijn, L., Grasmeijer, B., and Perk, L. (2018). Effect of channel deepening on tidal flow and sediment transport: part I – sandy channels. *Ocean. Dyn.* 68 (11), 1457–1479. doi:10.1007/s10236-018-1204-2

Verney, R., Deloffre, J., Brun-Cottan, J., and Lafite, R. (2007). The effect of wave-induced turbulence on intertidal mudflats: impact of boat traffic and wind. *Cont. Shelf Res.* 27 (5), 594–612. doi:10.1016/j.csr.2006.10.005

Wiberg, P., Taube, S., Ferguson, A., Kremer, M., and Reidenbach, M. (2019). Wave attenuation by oyster reefs in shallow coastal bays. *Estuaries Coasts* 42 (2), 331–347. doi:10.1007/s12237-018-0463-y

Williams, O. (Forthcoming 2022). *Evaluating living shoreline performance and vessel wake using the ship wake module of FUNWAVE-TVD*. master's thesis. Newark (DE): University of Delaware.

Zabawa, C., Kerhin, R., and Bayley, S. (1981). Effects of erosion control structures along a portion of the northern Chesapeake Bay shoreline. *Environ. Geol.* 3 (4), 201–211. doi:10.1007/bf02473504